Computer Physics Communications 80 (1994) 53–89
North-Holland

Computer Physics Communications

Transition matrix methods in atom–surface scattering theory

G. Armand
Service de Recherche sur les Surfaces et l'Irradiation de la Matière, Centre d'Études de Saclay, 91191 Gif-sur-Yvette, France
and
J.R. Manson
Department of Physics and Astronomy, Clemson University, Clemson, SC 29634, USA

A review of transition matrix methods as applied to the theory of atom–surface scattering at thermal energies is presented. The theory is applied to examples of elastic scattering, inelastic scattering, and scattering from defects and disorder on the surface.

1. Introduction

The scattering of thermal energy atoms from surfaces, and notably the scattering of He, is a well developed tool for obtaining detailed information on the structure and dynamics of surfaces [1]. Since the incident energies are small the method is totally non-destructive and the projectile samples only the outermost layer of the surface. In fact the incoming projectiles are reflected by the electronic density several atomic units in front of the first layer of surface atoms and hence the probe is a sensitive measure of the surface electron density. The scattered intensity consists of both elastic and inelastic contributions which can be distinguished with a time of flight energy sensitive detector. The elastic contribution contains diffraction peaks if the surface is sufficiently ordered, from which one can immediately determine the surface structure of the outermost layer. The inelastic contribution can exhibit sharp features due to the exchange of localised surface phonons, and from the positions and energies of these peaks the surface phonon dispersion relations are obtained. In the case of obtaining surface structure both from diffraction and phonon dispersion relations, little is needed in terms of theory since the positions of the relevant peaks are dictated by simple kinematics.

The atomic projectiles are very sensitive to small changes in the interaction potential because of the low energies involved, and hence the apparent cross section of a defect is quite large. Thus this type of experiment is extremely sensitive to defects on the surface, and a small coverage of defects gives rise to a significant diffuse background in the scattered intensity. Also, exchanges of multiple quanta of energy with the phonon field of the surface adds to the diffuse inelastic signal especially at higher temperatures, low mass ratios, and high incident energies.

In order to obtain the wealth of information available beyond simple structure or surface phonon dispersions, an adequate theory of the dynamics of the scattering process is required. Because of the

Correspondence to: G. Armand, Service de Recherche sur les Surfaces et l'Irradiation de la Matière, Centre d'Études de Saclay, 91191 Gif-sur-Yvette, France.

SSDI 0010-4655(93)E0100-2

many-body nature of the particle–surface interaction a complete theory is of necessity quite complicated and approximations must be made. There are a variety of different methods of approaching a general and complete theory of the scattering process, all of which are in principle equivalent [2]. The ultimate choice is predicated on considerations of ease of calculation and ability to effect the necessary approximations to the many-body processes.

In this paper we review the calculational approach based on transition matrix methods of scattering theory, which has been successfully applied to all of the aspects of the surface scattering problem, including problems of capture of particles into adsorbed states and consequent re-emission of adsorbed particles. In the next section we present the general formalism. In section 3 the general formalism is applied to the elastic scattering of a particle from a perfectly ordered surface. Section 4 is a treatment of scattering in the presence of defects on the surface. Section 5 gives the general formalism for treating the full dynamical many-body problem for inelastic scattering and energy exchange with the surface. Section 6 applies the inelastic formalism to the special case of thermal attenuation of the elastic diffraction intensities, and section 7 treats the exchange of energy between projectile and surface with emphasis on single-phonon scattering processes. Section 8 extends the inelastic many-body problem to questions of capture and sticking of the incoming particles.

2. General formalism

2.1. Schrödinger equation in integral form, and the T-matrix

In a scattering experiment, a particle beam is prepared far from the scattering center, approaches the crystal surface and is finally scattered into various final states via the particle–surface interaction potential. In a quantum description of this phenomenon, the particle is represented by an incident wave scattered by the potential into an outgoing wave which, asymptotically far from the surface, contains all the final states which may be reached by the incident particle. The theoretical problem consists of solving the Schrödinger equation given a well defined initial condition. In this kind of problem it is more convenient to start with the integral form of the Schrödinger equation in the two-potential formalism [3], which appears as

$$\Psi_i^+ = \Phi_i + G_0^+ (V - U) \Psi_i^+ . \tag{2.1}$$

The Green operator is given by

$$G_0^+ = (E_i - H_0 + \mathrm{i}\epsilon)^{-1}, \tag{2.2}$$

where E_i is the incident particle energy and H_0 is the distorted Hamiltonian given by the sum of the particle kinetic energy operator $-\hbar^2\nabla^2/2m$, with m the particle mass, the distorting potential $U(z)$, and the crystal Hamiltonian H_c. The distorting potential is chosen as close as possible to the interaction potential and in such a way that eigenvalues E_l and eigenvectors Φ_l of H_0 are known. The incident state Φ_i is one of the continuum states of the distorting potential, and reverts to the product of a sinusoidal standing wave and an unperturbed crystal state $|n_i\rangle$ at large distances from the surface.

Now the projection operator is introduced into eq. (2.1). Defining the reduced transition matrix element ${}_lT_i = \langle \Phi_l | (V - U) | \Psi_i \rangle$, one gets:

$$\Psi_i = \Phi_i + \sum_l \Phi_l \frac{1}{E_i - E_l + \mathrm{i}\epsilon} {}_lT_i, \tag{2.3}$$

an expression which shows that the unknown function is expanded in terms of the basis functions of H_0. However, the coefficient or amplitude of each partial wave Φ_l contains the unknown matrix element ${}_lT_i$. In order to obtain the equation giving these quantities one multiplies eq. (2.3) on the left by $\langle \Phi_f|(V-U)$. One gets

$$ {}_fT_i = \langle \Phi_f|(V-U)|\Phi_i\rangle + \sum_l \langle \Phi_f|(V-U)|\Phi_l\rangle \frac{1}{E_i - E_l + i\epsilon} {}_lT_i, \tag{2.4} $$

that is to say a set of coupled integral equations which gives formally the solution of the problem. It is convenient to define a new operator T such that

$$ \langle \Phi_l|T|\Phi_i\rangle = {}_lT_i = \langle \Phi_l|(V-U)|\Psi_i^+\rangle. \tag{2.5} $$

Then one can write the operator equation

$$ T = V + VG^+T. \tag{2.6} $$

Taking matrix elements of (2.6) and using the projection operator as above, the set of equations (2.4) above is easily recovered.

The transition matrix elements defined above have the dimension of energy. In the subsequent theoretical work it is more convenient to work with dimensionless quantities. Consequently, we consider a quantity χ having the dimensions of inverse length which is identified with the damping coefficient of the exponential tail of the repulsive part of the potential. Using the inverse energy

$$ A^2 = \frac{2m}{\hbar^2\chi^2}, \tag{2.7} $$

we define dimensionless energies according to $\tilde{E} = A^2E$, and the dimensionless transition matrix as $\tilde{T} = A^2T$. Dimensionless wave vectors are given by $\boldsymbol{p} = \boldsymbol{k}/\chi$, $p = k_z/\chi$.

2.2. Measurable quantities

In a typical scattering experiment, far from the surface where the interaction is negligible, the particle wave function consists of an incident plane wave φ_i with an amplitude usually taken to be unity, and outgoing scattered plane waves φ_q of varying amplitude. Since it is a practical impossibility to measure the complete quantum mechanical state of the crystal, the information obtainable about the structure and dynamics of the surface is contained in the amplitudes of the scattered plane waves. Depending upon experimental circumstances, the measurable quantities are:

(i) the reflection coefficient in the final state f, ${}_fR_i$, or the probability to find an incident particle in this final state This is measured or calculated by taking the ratio for the final to the incident state of particle flux in the direction normal to the surface. Thus we have

$$ {}_fR_i = \frac{J_f}{J_i}, \tag{2.8} $$

with

$$ J_q = \mathrm{Re}\left(\varphi_q^* \frac{\hbar}{im} \frac{\partial}{\partial z}\varphi_q\right); \tag{2.9} $$

(ii) the cross section:

$$\frac{\mathrm{d}_f R_i}{\mathrm{d}\Omega} = {}_f R_i d_f, \tag{2.10}$$

where d_f is the density of states in the small solid angle $\mathrm{d}\Omega$ surrounding the f state;

(iii) the transition rate ${}_f w_i$ defined as the number of particles undergoing transition from the state i to the state f per unit time. This is given by

$${}_f w_i = \frac{2\pi}{\hbar}\left|{}_f \mathsf{T}_i\right|^2 \delta(E_f - E_i), \tag{2.11}$$

in which the delta function insures the conservation of the total energy of the system studied (in this case, the energy of the crystal plus that of the particle). In (2.11) the symbol T stands for the full transition matrix as expressed in eq. (2.19) below. The transition rate is related to the reflection coefficient by the relation

$${}_f w_i = {}_f R_i J_i. \tag{2.12}$$

From the theoretical point of view we use these different quantities. For instance the transition rate is very useful for calculating the sticking or capture coefficient because this involves the transition between an incident and a bound state of the potential. Also the formulation of inelastic scattering is easier using the definition of the transition rate in eq. (2.11). On the other hand, the quantities ${}_f R_i$ or $d_f R_i/\mathrm{d}\Omega$ are usually measured in an experiment. The particle detector is located far from the scattering center and the flux J should be evaluated for large values of z. This implies obtaining an expression of the wave function Ψ_i in the asymptotic region of z going to infinity.

The eigenvectors of the Hamiltonian H_0 in the case of elastic scattering are

$$\Phi_i(\boldsymbol{R}, z) = B \exp(\mathrm{i}\boldsymbol{K}_i \cdot \boldsymbol{R})\phi_p(z), \tag{2.13}$$

where $\phi_p(z)$ are the eigenvectors of $U(z)$ and B is a normalisation factor. As usual, a vector $\boldsymbol{r}$ and a wave vector $\boldsymbol{k}$ are decomposed into components parallel to the surface represented by capital letters such as $[\boldsymbol{R}, \boldsymbol{K}]$ and components normal to the surface by lower case letters $[z, k_z]$. Introducing the corresponding projector in eq. (2.1) and taking account of the definition of the transition matrix element, one gets

$$\Psi_i^+ = B \exp(\mathrm{i}\boldsymbol{K}_i \cdot \boldsymbol{R})\ \phi_i(z) + \frac{B}{4\pi^2}\iint \mathrm{d}\boldsymbol{K} \exp(\mathrm{i}\boldsymbol{K} \cdot \boldsymbol{R}) \int_0^\infty \mathrm{d}p\ \phi_p(z) \frac{1}{\tilde{E}_i - \tilde{E}_p + \mathrm{i}\epsilon}{}_{K,p}\tilde{T}_i. \tag{2.14}$$

For $z \to \infty$, ϕ_p reduces to a standing wave $2\cos(p\chi z + \varphi)$. With these expressions the integration over p is readily done upon choosing an appropriate contour in the complex plane. One obtains

$$\Psi_i^+ = B \exp(\mathrm{i}\boldsymbol{K}_i \cdot \boldsymbol{R})\ \phi_i(z) + \frac{B}{4\pi^2}\iint \mathrm{d}\boldsymbol{K}_f \exp(\mathrm{i}\boldsymbol{K}_f \cdot \boldsymbol{R}) \exp\left(\mathrm{i}[\,p_f \chi z + \varphi_f\,]\right)\left(\frac{-\mathrm{i}\pi}{p_f}\right)_{K_f, p_f}\tilde{T}_i. \tag{2.15}$$

Now it becomes easy to calculate the reflection coefficient and the cross section since the evaluation of the constant B results in the general form $B^2 = \chi/2\pi$ [4]. The result is

(i) for reflection coefficient:

$${}_f R_i = \frac{\pi^2}{p_i p_f}\left|{}_f \tilde{T}_i\right|^2, \tag{2.16}$$

an expression valid whatever the final state may be, including diffraction states. However, for the specular peak we should take account of the first term of (2.15), and one gets:

$$ {}_sR_i = \left| 1 - \frac{i\pi_s \tilde{T}_i}{p_i} \right|^2 ; \tag{2.17} $$

(ii) for the cross section:

$$ \frac{dR}{d\Omega} = \frac{\pi^2}{\cos(\theta_i)} \frac{\left| {}_f\tilde{T}_i \right|^2}{A_G \chi^{-2}}, \tag{2.18} $$

where θ_i is the incident angle defined with respect to the surface normal and A_G is the unit cell surface area of a reciprocal lattice, that is to say of a lattice taken on the ideal periodic surface.

2.3. Unitary

It is of interest at this point to introduce a short discussion of unitarity and the optical theorem. Unitarity is, in essence, the statement that the total number of particles incident onto the surface equals the total number of scattered particles. This not only provides interesting mathematical relationships between the elements of the transition matrix, but it can also be verified experimentally [5].

The transition matrix in the two potential formalism is of the form [3]

$$ {}_f\mathsf{T}_i = \left(\varphi_f | U | \Phi_i^+\right) + \left(\Phi_f^- | V - U | \Psi_i^+\right) = \left(\varphi_f | U | \Phi_i^+\right) + {}_fT_i \tag{2.19} $$

and for a distorting potential describing a mirror surface, i.e., one which is flat $U = U(z)$ and totally reflecting, this becomes in dimensionless notation

$$ {}_f\tilde{\mathsf{T}}_i = i\frac{p_i}{\pi}\delta_{sf} + {}_f\tilde{T}_i, \tag{2.20} $$

where the symbol s signifies the unperturbed quantum state corresponding to the specular beam.

Two important elements of the transition matrix can be immediately evaluated. The transition matrix for forward scattering is

$$ {}_i\tilde{\mathsf{T}}_i = -i\frac{p_i}{\pi}, \tag{2.21} $$

which is exactly the value needed to cancel and extinguish the incident plane wave asymptotically deep under the surface. The transition matrix for specular scattering by the potential $U(z)$ is, from (2.19),

$$ \left(\varphi_s | U | \Phi_i^+\right) = i\frac{p_i}{\pi} e^{i\delta_i}. \tag{2.22} $$

The phase δ_i depends on the explicit form of $U(z)$, but with appropriate choice of the phase of the reduced transition matrix ${}_f\tilde{T}_i$ the phase δ_i can be ignored.

The optical theorem is most simply expressed as the following condition on the transition operator:

$$ \mathsf{T} - \mathsf{T}^+ = \mathsf{T}^+(\mathsf{G}^+ - \mathsf{G}^-)\mathsf{T}. \tag{2.23} $$

The most interesting statement arising from the optical theorem is that obtained upon taking diagonal matrix elements

$$ \mathrm{Im}\ {}_i\mathsf{T}_i = -\pi \sum_j \left| {}_j\mathsf{T}_i \right|^2 \delta(E_f - E_i). \tag{2.24} $$

For the moment we specialise to the case of elastic scattering, although the extension to the inelastic case involving energy exchange with the elementary excitations of the surface is straightforward. Then (2.24) becomes

$$\operatorname{Im} {}_i\tilde{\mathsf{T}}_i = -\tfrac{1}{2}\pi \sum_{\boldsymbol{K}} \frac{1}{p_{\boldsymbol{K}}} \left| {}_{\boldsymbol{K},p_{\boldsymbol{K}}}\tilde{\mathsf{T}}_i \right|^2, \tag{2.25}$$

where $p_{\boldsymbol{K}}$ is given by energy conservation.

Equation (2.25) is a statement of the optical theorem as it applies to the full ${}_f\tilde{\mathsf{T}}_i$ matrix. To obtain the corresponding expression for the reduced transition matrix ${}_f\tilde{T}_i$, we insert eq. (2.20) together with the known value of ${}_f\tilde{\mathsf{T}}_i$ from eq. (2.21), which leads to

$$\operatorname{Im} {}_s\tilde{T}_i = -\tfrac{1}{2}\pi \sum_{\boldsymbol{K}} \frac{1}{p_{\boldsymbol{K}}} \left| {}_{\boldsymbol{K},p_{\boldsymbol{K}}}\tilde{T}_i \right|^2. \tag{2.26}$$

There is an obvious connection between the optical theorem as expressed in eq. (2.24) and the transition rate (2.11) or reflection coefficient (2.12). The results of (2.26) can be readily shown to be equivalent to the unitarity statement that the sum of all reflection intensities is unity:

$$1 = \sum_{\boldsymbol{K}} {}_{\boldsymbol{K}}R_i. \tag{2.27}$$

2.4. *Two-potential decomposition*

It can be useful to decompose the total potential V into a sum of potentials, in such a way that, for each of them, the corresponding t matrix element could be calculated easily. We consider here the simplest case of decomposition, i.e.,

$$V = v_1 + v_2. \tag{2.28}$$

Then if h and t are respectively the T matrix elements for the scattering by v_1 and v_2, , i.e., the known solutions of

$$h = v_1 + v_1 G^+ h, \tag{2.29}$$

$$t = v_2 + v_2 G^+ t, \tag{2.30}$$

the solution of eq. (2.6) is given by [6]

$$T = h + s + hG^+ s + sG^+ h + hG^+ sG^+ h, \tag{2.31}$$

with

$$s = t + tG^+ hG^+ s. \tag{2.32}$$

This last equation, which should be solved, has the structure of a T matrix integral equation. However, the potential is replaced by the t matrix and the Green operator becomes a dressed Green operator equal to $G^+ hG^+$. In order to use this formalism in the case of scattering of a particle by a surface it is convenient to put

$$v_1 = V_s(\boldsymbol{R}, z) - U(z), \tag{2.33}$$

where $V_s(\boldsymbol{R}, z)$ is the periodic potential of the ideal surface yielding diffraction phenomena. For elastic

calculation this is the primitive surface potential. In the case of inelastic calculations the total potential depends also on the phonon displacement operator $\boldsymbol{u}$. V_s may be chosen equal to

$$V_s = \langle\langle V(\boldsymbol{R}, z, \boldsymbol{u})\rangle\rangle, \tag{2.34}$$

the thermal average of the potential over the vibrational states of the crystal. Then $U(z)$ is taken equal to the zero-order Fourier component of V_s, and

$$G^+ = G_0^+ = \left(E_i - \frac{\hbar^2}{2m}\Delta - U(z) + i\epsilon\right)^{-1}. \tag{2.35}$$

In each kind of calculation, the corresponding h matrix element could be obtained following the prescription exposed in section 3 below. Then, v_2 is equal to the difference between the two potentials V and V_s, the last one being in any case a static and periodic potential.

3. Elastic diffraction

One of the most important problems to be addressed by surface scattering theory is the diffraction of the incident beam by a perfectly periodic and rigid surface. The surface is represented by a potential $V(\boldsymbol{R}, z)$ which can be expanded in a Fourier series in the reciprocal lattice vectors $\boldsymbol{G}$ in the directions parallel to the surface

$$V(\boldsymbol{R}, z) = \sum_{\boldsymbol{G}} e^{i\boldsymbol{G}\cdot\boldsymbol{R}} V_{\boldsymbol{G}}(z). \tag{3.1}$$

The conditions for diffractive scattering are expressed in the kinematical equations of conservation of energy

$$E_f = E_i \tag{3.2}$$

and parallel momentum

$$\boldsymbol{K}_f = \boldsymbol{K}_1 + \boldsymbol{G}, \tag{3.3}$$

which are recognised as the conditions for diffraction from a two-dimensional periodic grating.

The Schrödinger equation for this potential is

$$-\frac{\hbar^2}{2m}\left(\frac{\partial^2}{\partial z^2} + \nabla_{\boldsymbol{R}}^2\right)\Psi_i(\boldsymbol{R}, z) + V(\boldsymbol{R}, z)\,\psi_i(\boldsymbol{R}, z) = E_i\Psi_i(\boldsymbol{R}, z) \tag{3.4}$$

and the periodicity of the potential implies that the wave function can be written as a Bloch function in the parallel direction as

$$\Psi_i(\boldsymbol{R}, z) = \sum_{\boldsymbol{G}} e^{i(\boldsymbol{K}_i+\boldsymbol{G})\cdot\boldsymbol{R}}\Psi_{k_{G,z}}(z), \tag{3.5}$$

where $k_{Gz}^2 = k_i^2 - (\boldsymbol{K}_i + \boldsymbol{G})^2$. Equations (3.1) and (3.5) allow the Schrödinger equation to be written as a set of linear coupled differential equations in the $\Psi_{kG,z}(z)$:

$$-\frac{\hbar^2}{2m}\frac{\partial^2}{\partial z^2}\Psi_{k_{G,z}}(z) + \sum_{\boldsymbol{G}'} V_{\boldsymbol{G}-\boldsymbol{G}'}(z)\,\Psi_{k_{G'z}}(z) = \frac{\hbar^2}{2m}k_{G,z}^2\Psi_{k_{G,z}}(z). \tag{3.6}$$

The form of the set of equations (3.6) bears some resemblance to the coupled equations for rotational and vibrational states that arises in atomic and molecular scattering and which are often solved by the close coupling method. Wolken first adapted the close coupling method, essentially a direct integration in real space, to the set (3.6) [7] and this method remains one of the most utilised methods of solution. The major disadvantage with the close coupling method is that it takes a prohibitive amount of computer time for surfaces with large unit cells and consequently large numbers of diffraction peaks.

Efficient methods of solving the elastic diffraction problem can be based on the transition matrix equation. The only scattering channels are the diffraction beams, and the transition matrix equation becomes a linear set of coupled equations. For computational purposes it is more appropriate to work in the distorted wave formalism, and the logical choice (although certainly not the only choice) for the distorting potential $U(z)$ is

$$U(z) = V_{G=0}(z), \tag{3.7}$$

which leaves for the perturbing potential $v(\boldsymbol{R}, z)$

$$v(\boldsymbol{R}, z) = \sum_{G \neq 0} e^{iG \cdot R} v_G(z). \tag{3.8}$$

The transition matrix in the dimensionless two-potential formalism is then

$$_{G,k_{G,z}}\tilde{T}_i = i\frac{p_i}{\pi}\delta_{G0} + {}_{G,k_{G,z}}\tilde{T}_i, \tag{3.9}$$

with the reduced transition matrix given by the linear set of coupled equations

$$_{G,p_G}\tilde{T}_i = {}_{G,p_G}\tilde{v}_i + \frac{1}{2\pi}\sum_{G'}\int_0^\infty dp' \; {}_{G,p_G}\tilde{v}_{G',p'}\frac{1}{p_{G'}^2 - p'^2 + i\epsilon}\,{}_{G',p'}\tilde{T}_i + \sum_{G'}\sum_b {}_{G,p_G}\tilde{v}_{G',b}\frac{1}{p_{G'}^2 - p_b^2}\,{}_{G',b}\tilde{T}_i. \tag{3.10}$$

The final term on the right-hand side of eq. (3.10) is the discrete sum over bound states in the adsorption well of the potential. These bound states have negative energies for motion in the direction normal to the surface, hence the p_b^2 are negative definite. The integral over normal momenta in eq. (3.10) must also be separated into the principal part and the pole contributions according to

$$\begin{aligned} _{G,p}\tilde{T}_i = {}_{G,p}\tilde{v}_i - i\sum_{G'}\frac{1}{4p_{G'}}\,{}_{G,p_G}\tilde{v}_{G',p_{G'}}\,{}_{G',p_{G'}}\tilde{T}_i + \frac{1}{2\pi}\sum_{G'}\mathrm{P}\int_0^\infty dp' \; {}_{G,p_G}\tilde{v}_{G',p'}\frac{1}{p_{G'}^2 - p'^2}\,{}_{G',p'}\tilde{T}_i \\ + \sum_{G'}\sum_b {}_{G,p_G}\tilde{v}_{G',b}\frac{1}{p_{G'}^2 - p_b^2}\,{}_{G',b}\tilde{T}_i. \end{aligned} \tag{3.11}$$

This set is completely equivalent to the coupled channel equations of (3.4) above.

Equation (3.11) has been solved by direct matrix inversion [8], (see the appendix). This is accomplished by discretising the integral over normal momentum in the principal part integral. The resulting matrix equation is directly inverted, and this process is numerically possible to carry out with systems having more than 20 diffraction peaks using large computers [9].

A second way to solve the diffraction problem is by obtaining the reduced transition matrix $_{G,p_G}\tilde{T}_i$ by summing the distorted wave perturbation series. This is equivalent to solving (3.11) by iteration, and symbolically what is done is to sum the series

$$\tilde{T} = \tilde{v} + \tilde{v}G\tilde{v} + \tilde{v}G\tilde{v}G\tilde{v} + \cdots \tag{3.12}$$

until the result for ${}_{G,p_G}\tilde{T}_i$ converges to a sufficiently precise value. Although there is no proof that the perturbation series summation is convergent, it has been demonstrated with numerous examples that quite satisfactory results can be obtained with this method, even for surfaces with relatively large corrugations [4,10–12]. Sometimes, however, the numerical convergence of the result is more rapid for choices of the distorting potential $U(z)$ other than that suggested by eq. (3.5) [11].

In the case of selective adsorption resonance with the bound states, the associated energy denominators in the summation over the bound states in eqs. (3.10) or (3.11) becomes vanishingly small. In order to avoid this inconvenient numerical difficulty the discrete number of bound states in resonance are projected out of eq. (3.11) and the iteration process is carried out on the resulting reduced set of coupled transition matrix equations similar to that described in section 2.4 above [11]. The convergence properties of the equations for diffraction remain the same both near and away from conditions of resonance.

There is a second class of resonances which can occur in atom–surface scattering known as threshold resonances [13,14]. These resonances occur when the incident conditions are such that a new diffraction peak is just emerging from the surface at grazing scattering angle. Such new peaks grow rapidly in intensity as they emerge, and this rapid growth results in a redistribution of intensity among the other diffraction beams. Threshold resonances are normally not an important effect in He-surface scattering, but under some circumstances they are observable. They do not cause any special calculational difficulties.

In general, the methods based on the solution of the transition matrix equation are considerably more rapid than the close coupling formalism for systems with larger numbers of important diffraction peaks. This is because the close coupling formalism supplies a solution to the complete boundary value problem, which means that the solution can be used to obtain diffraction amplitudes for all possible initial or final conditions imposed on the system. The two methods described here, based on the T matrix equations, give initial value solutions, i.e., they give the diffraction intensities for only a single specified initial condition.

4. Elastic scattering from surfaces with defects

On the surface of a real crystal, there are always adsorbed atoms or molecules, and/or vacancies, steps, etc. Generally speaking there are always what we shall call surface defects, which destroy the periodicity of the primitive, ideal surface. The measured cross section [15,16] of these defects are of the order of 60 to 200 Å^2, i.e., large compared to a surface unit cell. It follows that, before performing a diffraction experiment, it is necessary to be very careful with the crystal preparation, in order to reduce the quantity of surface defects to as small a level as possible. However, even if this appears as a drawback in diffraction studies, it becomes an advantage in the experimental study of surface defects. Hence, the scattering of atoms or light molecules is a powerful tool in the study of defect distributions on surfaces or in the modification of surface structure as happens in the case of surface reconstruction or surface roughening. So it becomes necessary to have a reliable theory of the scattering phenomena by a surface on which the perfect periodicity has been destroyed by the surface defects. With this in mind, we build a surface model starting with a given periodic surface on which are added some defects with a given distribution. From a theoretical point of view, they will add to the periodic potential an additional potential considered as a perturbation.

4.1. Model

On the sites of the periodic surface, for instance the different unit cells for the case of a P (1×1) structure, are adsorbed some defects, i.e., adatoms or advacancies. For sake of simplicity, we suppose

that all the defects are of the same nature. The case of two kinds of adsorbed defects as well as the case of defects gathered in domains, has been also treated in previous publications [17,18], from which furthermore, we draw out the results presented in the three following subsections [18]. To each unit cell is attached a variable x_d equal to 0 or 1 according to whether the corresponding adsorption site is vacant or occupied. Note that the average of x_d, over the different configurations, at constant number of impurities, is equal to the coverage:

$$\{x_d\} = \theta. \tag{4.1}$$

This relation holds, whatever the distribution of impurities may be.

Following the decomposition of the potential exposed in section 2.4, v_1 is defined by eq. (2.33). The solution of the attached eq. (2.29) gives the set of diffraction peak amplitudes denoted by ${}_G h_i$, where $\boldsymbol{G}$ refers to a reciprocal lattice vector of the periodic surface. The other component of the potential v_2 is equal to:

$$v_2 = V(\boldsymbol{R}, z) - V_s(\boldsymbol{R}, z), \tag{4.2}$$

i.e., the potential added by the adsorbed impurities. We assume that this difference is given by a sum of two-body potentials, each impurity giving a contribution v_d. Hence one writes

$$v_2 = \sum_d x_d v_d. \tag{4.3}$$

The periodicity or the symmetry of the potential being broken, the set of open channels for the scattered particle is composed of an infinite set of pairs $(\boldsymbol{K}, k_z)$ and $(\rho = |\boldsymbol{K}|/\chi, \Omega_b)$ where $\Omega_b = -A^2 e_b$, is equal to the dimensionless value of a bound states energy e_b of $U(z)$, provided they satisfy the conservation of energy relations:

$$\boldsymbol{p}^2 = \rho^2 + p^2 \quad \text{or} \quad \boldsymbol{p}^2 = \rho^2 + \Omega_b. \tag{4.4}$$

4.2. T matrix elements

Equation (4.3) indicates that v_2 is given by a sum over all the surface unit cells of a potential attached to each of them. The procedure exposed in section 2.4 can be extended to three, four, or any number of components of the potential. In this way it is demonstrated in ref. [18] that the matrix s is given by the relation

$$s = \sum_d x_d s_d, \tag{4.5}$$

where the s_d are given by the coupled set of equations:

$$s_d = t_d + t_d G_0^+ h G_0^+ s + t_d G_0^+ \sum_{d'} s_{d'}(1 - \delta_{d,d'}), \tag{4.6}$$

with

$$t_d = v_d + v_d G_0^+ t_d, \tag{4.7}$$

while the T matrix is always given by eq. (2.31). Hence the s matrix is calculated with the set of s_d submatrices, themselves solutions of the set of eq. (4.6). In this set the basic quantities are the t_d matrix of eq. (4.7) which depicts the scattering by the potential $U(z) + v_d(\boldsymbol{R}_d, z)$, i.e., particles scattered by one impurity located on the unit cell d of a flat surface.

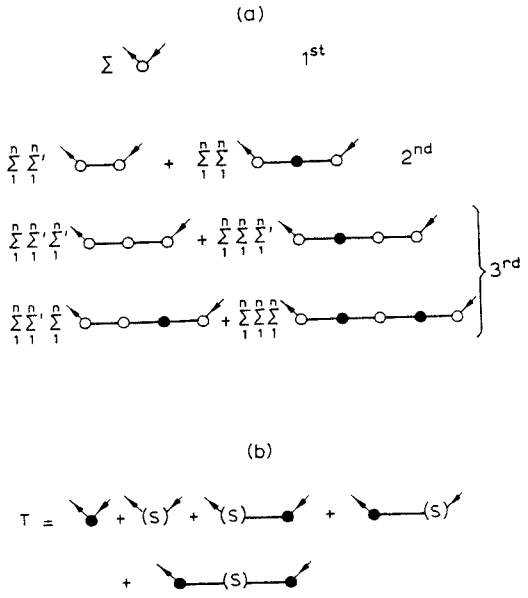

Fig. 1. (a) Diagrams corresponding to the iteration of s matrices up to 3rd order. (b) Total T matrix. Open circles represent scattering by a defect located on a flat surface. Solid circles represent scattering by the perfect periodic surface (diffraction). A solid line represents the elastic Green operator.

The physical meaning of the t_d matrix is now clear. In order to look at those elements of s we consider the different iteration steps of eq. (4.6). At the first order we get

$$s_d = t_d, \qquad s^{(1)} = \sum_d x_d t_d, \tag{4.8}$$

where $s^{(1)}$ is the sum of the scattered amplitude yielded by each of the defects located on the flat surface. The second-order term is equal to:

$$s^{(2)} = s^{(1)} + \sum_d \sum_{d'} x_d x_{d'} \left(t_d G_0^+ h G_0^+ t_{d'} + t_d G_0^+ t_{d'} (1 - \delta_{d,d'}) \right) \tag{4.9}$$

and adds two terms, each of them being a sum over all the defect pairs, with permutation of order in each pair with respect to incident and final states. The first one, under the summations, describes a particle scattered by defect d' followed by diffraction on the perfect surface and finally scattered by defect d. The second one represents the double scattering on a pair of defects excluding the scattering on pairs formed by a defect and itself, as these scattering events are already contained in t_d.

In fig. 1a, these different processes are represented by diagrams, up to third order of iteration. Usually in diagrams a point is equivalent to a matrix element of the potential and the propagator such as G_0^+ is represented by a line. As t_d and h contain multiple scattering events, we change the notation and they are represented by a white "○" and a black "●" circle, respectively. A primed sum Σ' indicates that the term $d = d'$ should be equal to zero, an occurrence which appears when there are two successive white circles.

As eq. (4.6) contains three terms, the iteration step of order n will add 2^{n-1} terms, each of them being composed of n sums. Therefore each component of these sums will contain the product of n variables such as x_d. This will yield, as we will see in the intensity or cross section expressions, the appearance of

the correlation function of defect positions. Also note that they begin and end with a white circle, i.e., the scattering process begins and ends on a defect.

Figure 1b represents the total T matrix eq. (2.31). The physical meaning of the first two diagrams is quite clear. The third one describes a particle first diffracted by the periodic potential and secondly scattered by the set of defects (s matrix). The fourth one describes the reverse process and the last is a combination of the two preceding ones.

4.3. Explicit expression and solution of the t_d matrix

The t_d matrix describes the scattering by a defect located on the flat surface at $\boldsymbol{R}_d$. With the equation of definition (2.5) and the set of eigenfunctions of $U(z)$ (2.13), it is easy to show that the corresponding dimensionles ${}_f(\tilde{t}_d)_i$ matrix elements is equal to:

$$ {}_f(\tilde{t}_d)_i = \exp(-\mathrm{i}\,{}_f\boldsymbol{Q}_i \cdot \boldsymbol{R}_d)\, {}_f\tilde{t}_i, \tag{4.10} $$

with ${}_f\boldsymbol{Q}_i = \boldsymbol{K}_f - \boldsymbol{K}_i$ the difference of parallel momentum between initial and final states, and ${}_f\tilde{t}_i$ the matrix element for the same impurity but now positioned at the origin. As indicated above, for sake of simplicity, we suppose that the impurities are of the same nature. Thus the dependence of ${}_f(\tilde{t}_d)_i$ upon the site d is entirely contained in the phase factor.

Now, dropping the subscript d in eq. (4.7), and taking the matrix element between incident $(\boldsymbol{K}_i, p_i)$ and final $(\boldsymbol{K}_f, p_f)$ states on each side, and using the projection operator, one gets

$$ {}_f\tilde{t}_i = {}_f\tilde{l}_i + \frac{A_c}{4\pi^2} \int \mathrm{d}\boldsymbol{K} \left(\int_0^\infty \frac{{}_f\tilde{l}_{\boldsymbol{K},q}\, {}_{\boldsymbol{K},q}\tilde{t}_i}{p_{\boldsymbol{K}}^2 - q^2 + \mathrm{i}\epsilon}\, \mathrm{d}q + \sum_b \frac{{}_f\tilde{l}_{\boldsymbol{K},b}\, {}_{\boldsymbol{K},b}\tilde{t}_i}{p_{\boldsymbol{K}}^2 + \Omega_b + \mathrm{i}\epsilon} \right), \tag{4.11} $$

with A_c the unit cell area, $p_{\boldsymbol{K}}^2 = p_i^2 - \rho^2$, and

$$ {}_f\tilde{l}_{\boldsymbol{K},q \text{ or } b} = \langle \Phi_f | \tilde{v}(\boldsymbol{R}, z) | \Phi_{\boldsymbol{K},q \text{ or } b} \rangle. \tag{4.12} $$

This equation is similar to that giving the matrix elements for the diffraction phenomena eq. (3.10). However, the discrete sum over reciprocal lattice vectors is replaced by an integral over the $\boldsymbol{K}$ plane, meaning that all the corresponding channels, open or closed, are attainable. Also the integration yields the disappearance of singularities or resonances which occurs when the denominator $p_{\boldsymbol{K}}^2 + \Omega_b$ vanishes. Here these conditions correspond to open channels such that

$$ \rho_r^2 = \boldsymbol{p}_i^2 + \Omega_b \tag{4.13} $$

and are located in the $\boldsymbol{K}$ plane, on the circle of radius ρ_r. The amplitude attached to the scattering in these channels is given by ${}_f\tilde{t}_i$ with a final state $(|\boldsymbol{K}_f| = \chi\rho_r, \Omega_b)$ to which corresponds a cross section.

In order to carry out numerical calculations, we assume that the potential $\tilde{v}$ of one impurity has the symmetry of revolution with respect to the variable $\boldsymbol{R}$. This is the case for an adatom or an advacancy. Then the $\tilde{t}$ equation is written in cylindrical coordinates and by discretisation of the integrals, is transformed into a set of linear equations. This procedure has been exposed in the case of diffraction in section 3 above, and will be detailed in a forthcoming publication [19]. Due to the great number of open and closed channels retained in the linear equations, the size of matrices to be inverted is of the order of 2000. This can be achieved only with big computers such as a CRAY2 as it demands about 125 MB of memory. The time involved is of the order of 100 minutes.

4.4. Explicit evaluation of ${}_f(\tilde{h}\tilde{G}_0^+\tilde{s})_i$

Keeping in mind that the initial state, referred to as i, is the state $(\boldsymbol{K}_i, p_i)$, the matrix element of $\tilde{h}$ can be written as

$$_{\boldsymbol{K},p}\tilde{h}_i = \frac{4\pi^2}{A_c}\sum_{\boldsymbol{G}}\delta(\boldsymbol{K}-\boldsymbol{K}_i-\boldsymbol{G})_{G,p_G}\tilde{h}_i. \tag{4.14}$$

Using this expression the matrix element ${}_f(hGs)_i$ can be calculated easily. One gets:

$$_f\left(\tilde{h}\tilde{G}_0^+\tilde{s}\right)_i = \sum_{\boldsymbol{G}}\left(\int_0^\infty \frac{_{\boldsymbol{K}_f,p_f}\bar{h}_{\boldsymbol{K}_f+\boldsymbol{G},q\ \boldsymbol{K}_f+\boldsymbol{G},q}\bar{s}_i}{p_f^2-q^2+i\epsilon}\,dq + \sum_b \frac{_{\boldsymbol{K}_f,p_f}\tilde{h}_{\boldsymbol{K}_f+\boldsymbol{G},b\ \boldsymbol{K}_f+\boldsymbol{G},b}\tilde{s}_i}{p_f^2+\Omega_b}\right). \tag{4.15}$$

One will find the complete expressions for ${}_f(\tilde{s}\tilde{G}_0^+\tilde{h})_i$ and ${}_f(\tilde{h}\tilde{G}_0^+\tilde{s}\tilde{G}_0^+\tilde{h})_i$ in ref. [18]. In a straightforward way, one can note that the first of these terms is essentially given by eq. (4.15) in which the order of $\tilde{h}$ and $\tilde{s}$ has been inverted. The second one can be established by putting the projector P in between $\tilde{s}$ and G_0^+, i.e., an expression which shows clearly that the particle is first scattered in the diffraction states and secondly undergoes the process described by eq. (4.15).

4.5. Intensities and cross sections

The reflection coefficient for diffraction peaks or the cross section for incoherent scattering should be calculated with the relations (2.16), (2.17) and (2.18), respectively. All of them are given by the product of a kinematical factor with $\left|{}_f\tilde{T}_i\right|^2$. The evaluation of ${}_f\tilde{T}_i$ leads to an expression which contains the whole set of the variables x_d. A given numerical set describes a given defect configuration. On the other hand, to each particle in an experiment is associated a coherence length and consequently it probes a limited area on the surface. In the beam the different particles probe different areas or defect configurations on the surface and, on the whole, the beam views an average over the defect configurations. Therefore, in order to compare the calculated results to experimental data it is necessary to calculate the average of the square modulus of ${}_f\tilde{T}_i$, denoted as $\{\left|{}_f\tilde{T}_i\right|^2\}$. This will be used in the above referred expressions in place of $\left|{}_f\tilde{T}_i\right|^2$.

4.5.1. First-order perturbation

At this point, combining eq. (4.8) and (4.10), one gets

$$_f\tilde{s}_i^{(1)} = {}_f\tilde{t}_i\sum_d x_d\,\exp(-i_f\boldsymbol{Q}_i\cdot\boldsymbol{R}_d). \tag{4.16}$$

This value is introduced in eq. (2.31) which yields the T matrix element to first order ${}_f\tilde{T}_i^{(1)}$. Before writing its expression it is worthwhile to remark that the sum Σ_d factorises also into each of its three last terms. For instances, eq. (4.15) is now written as

$$_f\left(\tilde{h}\tilde{G}_0^+\tilde{s}^{(1)}\right)_i = {}_f\left(\tilde{h}\tilde{G}_0^+\tilde{t}\right)_i\sum_d x_d\,\exp(-i_f\boldsymbol{Q}_i\cdot\boldsymbol{R}_d). \tag{4.17}$$

Then one gets

$$_f\tilde{T}_i^{(1)} = \sum_{\boldsymbol{G}}{}_G\tilde{h}_i\delta_{Q,G} + \left(\sum_d x_d\,\exp(-i_f\boldsymbol{Q}_i\cdot\boldsymbol{R}_d)\right){}_f\tilde{F}_i^{(1)}, \tag{4.18}$$

with

$$ {}_f\tilde{F}_i^{(1)} = {}_f\tilde{t}_i + {}_f\left(\tilde{h}\tilde{G}_0^+\tilde{t}\right)_i + {}_f\left(\tilde{t}\tilde{G}_0^+\tilde{h}\right)_i + {}_f\left(\tilde{h}\tilde{G}_0^+\tilde{t}\tilde{G}_0^+\tilde{h}\right)_i . \tag{4.19} $$

Therefore, for incoherent scattering the cross section will be proportional to

$$ \left\langle \left| {}_f\tilde{T}_i^{(1)} \right|^2 \right\rangle = \left(\sum_d \sum_{d'} \{x_d x_{d'}\} \exp\left(-\mathrm{i}_f \boldsymbol{Q}_i \cdot (\boldsymbol{R}_d - \boldsymbol{R}_{d'}) \right) \right) \left| {}_f\tilde{F}_i^{(1)} \right|^2 , \tag{4.20} $$

a quantity equal to the product of a structure factor and of a form factor. The former depends on the defect statistics through the two-body correlation function of position. The latter, $\left| {}_f\tilde{F}_i^{(1)} \right|^2$, depicts the scattering of the particle by one defect located on the primitive and periodic surface.

In the structure factor the correlation function value depends upon the distance between cells d and d'. At very large distance, we expect that the two defects become decorrelated. This is certainly true when the forces between adspecies are purely attractive. Then the correlation function becomes equal to $\{x_d\}^2$, i.e., equal to θ^2. The correlation function can be written as

$$ \left(\{x_d x_{d'}\} - \theta^2 \right) + \theta^2 \tag{4.21} $$

and the term in parenthesis will yield incoherent scattering, while the other contributes to diffraction peak intensities which are δ functions. One gets the following results.

4.5.1.1. The coherent or diffraction peak intensities

$$ {}_G R_i^{(1)} = {}_G R_i^{(0)} + \frac{\pi^2}{p_i p_{\boldsymbol{K}_i + \boldsymbol{G}}} \left(2\theta \ \mathrm{Re}\left({}_{\boldsymbol{K}_i+\boldsymbol{G}}\tilde{h}_i^* \ {}_{\boldsymbol{K}_i+\boldsymbol{G}}\tilde{F}_i^{(1)} \right) + \theta^2 \left| {}_{\boldsymbol{K}_i+\boldsymbol{G}}\tilde{F}_i^{(1)} \right|^2 \right) \tag{4.22} $$

and for the special case of the specular beam

$$ {}_i R_i^{(1)} = {}_i R_i^{(0)} + \frac{2\pi}{p_i}\theta \ \mathrm{Im}\left({}_i\tilde{F}_i^{(1)} \right) + \frac{\pi^2}{p_i^2} 2\theta \ \mathrm{Re}\left({}_i\tilde{h}_i^* \ {}_i\tilde{F}_i^{(1)} \right) + \frac{\pi^2}{p_i^2}\theta^2 \left| {}_i\tilde{F}_i^{(1)} \right|^2 , \tag{4.23} $$

where in this formula ${}_G R_i^{(0)}$ corresponds to the diffraction intensity for the bare or perfect surface. It is important to remark that these coherent intensities do not depend upon the defect distribution on the surface but only upon the coverage θ. This is a particularity of the first-order terms. They are function of θ and θ^2 and can increase or decrease with the coverage depending whether the sign of the term multiplying θ is positive or negative, respectively. For most cases $\mathrm{Im}({}_i\tilde{F}_i^{(1)})$ and $\mathrm{Im}({}_i\tilde{h}_i)$ are negative, but one cannot predict the sign of $\mathrm{Re}(h^*F)$.

As previously defined by the experimentalists for the specular intensity, one can also define a defect cross section for each diffracted beam $\boldsymbol{G}$, denoted as Σ_G:

$$ \Sigma_G = \left(\frac{\mathrm{d}_G R_i}{\mathrm{d}\theta} \right)_{\theta=0} \left({}_G R_i^{(0)} \right)^{-1} . \tag{4.24} $$

They are equal to

$$ \Sigma_{G\neq 0}^{(1)} = \frac{\pi^2}{p_i p_{\boldsymbol{K}_i+\boldsymbol{G}}} \left(2 \ \mathrm{Re}\left({}_{\boldsymbol{K}_i+\boldsymbol{G}}\tilde{h}_i^* \ {}_{\boldsymbol{K}_i+\boldsymbol{G}}\tilde{F}_i^{(1)} \right) \right) \left({}_G R_i^{(0)} \right)^{-1} , \tag{4.25} $$

and for the specular beam

$$\Sigma_i^{(1)} = \left(\frac{2\pi}{p_i} \mathrm{Im}\left({}_i\tilde{F}_i^{(1)}\right) + \frac{\pi^2}{p_i^2} 2\ \mathrm{Re}\left({}_i\tilde{h}_i^*\ {}_i\tilde{F}_i^{(1)}\right) \right) \left({}_iR_i^{(0)}\right)^{-1}. \tag{4.26}$$

For a given kind of defect these values depend on the corrugation of the perfect surface on which the defects are adsorbed through the ${}_Gh_i$ values and therefore, for a given surface depend on the order of the diffraction peak.

On the dense faces, such as the (111) or (100) crystallographic plane, the diffraction peaks are very small and the corresponding matrix elements of h have negligible values. In this case the intensities or the cross section are given by the above formula in which the h values are taken equal to zero and ${}_iR_i^{(0)} = 1$. Therefore:

(i) the diffracted intensities increases as θ^2 and some of them could become measurable, especially those of lower order;

(ii) the specular intensity decreases as $\mathrm{Im}({}_i\tilde{F}_i^{(1)})$ is negative. The defect cross section is negative also;

(iii) comparing the cross section values for the flat and corrugated surface one finds $|\Sigma_i^{(1)}|$ on the flat surface $\geq |\Sigma_i^{(1)}|$ on the corrugated surface.

4.5.1.2. The incoherent cross section

Assuming stationary conditions for the defect statistics, one gets

$$\frac{\mathrm{d}R^{(1)}}{\mathrm{d}\Omega} = \frac{\pi^2}{\cos(\theta_i)\ A_G \chi^{-2}} \mathrm{TF}^{(2)}({}_f\boldsymbol{Q}_i) \left| {}_f\tilde{F}_i^{(1)} \right|^{(2)}, \tag{4.27}$$

with, $\boldsymbol{R}_0$ being the origin of the lattice sites of defects:

$$\mathrm{TF}^{(2)}({}_f\boldsymbol{Q}_i) = \sum_d \exp\left[-\mathrm{i}\,{}_f\boldsymbol{Q}_i \cdot (\boldsymbol{R}_d - \boldsymbol{R}_0) \right] (\{x_d x_0\} - \theta^2). \tag{4.28}$$

This last term is the structure factor equal to the discrete Fourier transform of the correlation function from which its large distance value has been subtracted. We outline its properties:

(i) its value is real because the correlation function is symmetric:

$$\{x_d x_0\} = \{x_{d'} x_0\} \quad \text{for} \quad \boldsymbol{R}_{d'} - \boldsymbol{R}_0 = -(\boldsymbol{R}_d - \boldsymbol{R}_0);$$

(ii) it is periodic on the reciprocal lattice $\boldsymbol{G}$ as the exponential term is invariant under the change $\boldsymbol{K}_f \to \boldsymbol{K}_f + \boldsymbol{G}$ for any $\boldsymbol{G}$ vectors;

(iii) as $\{x_d x_0\}$ is always positive, it has maxima for all ${}_f\boldsymbol{Q}_i = \boldsymbol{G}$.

(iv) for a random distribution it is equal to $\theta(1-\theta)$, as there is no correlation.

The form factor $\left| {}_f\tilde{F}_i^{(1)} \right|^2$ gives the intensity for the scattering by one defect on the primitive surface. It has also certainly maxima in the vicinity of the most intense diffraction peaks, because the terms ${}_f(\tilde{h}\tilde{G}_0^+\tilde{s})_i + \cdots$ couple diffraction and defect scattering, and is expected to vary smoothly between them. On the whole, one can expect to observe an incoherent pattern which exhibits the periodicity of the primitive lattice with the greatest intensity measured near the most intense diffraction peaks. Figure 2 depicts a qualitative representation of this pattern.

The case of a random distribution of defects is particular. As the structure factor is constant, the measurement of the incoherent intensities gives, apart from a factor of proportionality, the values of

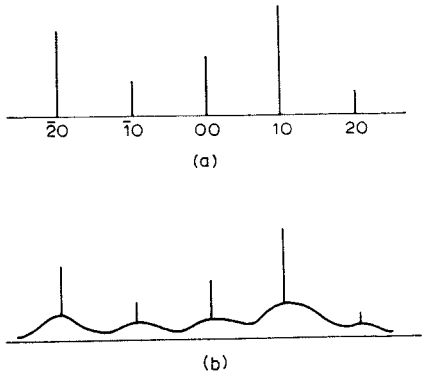

Fig. 2. Schematic representation of a scattering pattern: (a) perfect or primitive surface; (b) the above surface with defects (p (1×1) lattice sites).

$\left|{}_f\tilde{F}_i^{(1)}\right|^2$, i.e., the scattering pattern yielded by one defect on the primitive surface, as we have already outlined. The corresponding experimental situation appears at the onset of an adsorption process on a crystal of temperature sufficiently low to avoid adatom displacement. Once this measurement is done, one can increase the crystal temperature to a value for which the adatom mobility allows thermodynamic equilibrium to be achieved, without changing the coverage. Then the ratio of the two measurements gives the $\mathrm{TF}^{(2)}({}_f\boldsymbol{Q}_i)$ values, corresponding to the equilibrium distribution of defects.

4.5.2. Higher-order perturbations

The second order of iteration (eq. (4.9)) adds to the first order, a term which contains a double sum over the variables x_d attached to each unit cell. The resulting $\{\left|{}_f\tilde{T}_i^{(2)}\right|^2\}$ value will contain the correlation functions up to four bodies. The new expressions for the diffraction peak intensities and incoherent cross sections are a little more complicated, and are given in ref. [18]. Here it is sufficient to outline that:

(i) The diffraction peak intensities are given by a polynomial of degree four in θ.

(ii) There is no simple expression for the defect cross section $\Sigma_G^{(2)}$. However for a random distribution the calculation can be performed, and the results show that the difference $\Sigma_G^{(2)}-\Sigma_G^{(1)}$ is due to multiple scattering between the periodic lattice and the defects. Therefore, for a flat surface, this difference vanishes and the $\Sigma_G^{(1)}$ expression gives the exact value of the defect cross section.

(iii) The incoherent cross section expression is composed of three terms, each one containing respectively the Fourier transform of two-, three-, and four-body correlation functions. But the second and the third terms cannot be decomposed, as the first, into a product of structure and form factors, because the corresponding Fourier transforms are functions of the $\boldsymbol{K}$ variable and remain in the subsequent integrations over $\boldsymbol{K}$ space.

For higher order in the iteration expansion, say for order n, the term added to $\tilde{s}^{(n-1)}$ will contain n sums over the x_d variables. The diffracted intensities will be given by a polynomial of order n in θ. The incoherent cross section expressions will contain the Fourier transform of correlation functions up to $2n$ bodies. Hence, on the whole, the iteration procedure expresses the incoherent cross section as an expansion over the set of correlation functions. As this set is in principle necessary to describe the defect statistics, the whole iteration expansion takes account of all the properties of the defect distribution.

5. Inelastic scattering–general theory

5.1. General expressions [20]

The potential V depends now on the crystal atom displacement operator $\boldsymbol{u}$. As explained in section 2.4 we take the following potential decomposition,

$$v_1 = \langle\langle V(\boldsymbol{R}, z, \boldsymbol{u})\rangle\rangle - U(z), \qquad v_2 = V(\boldsymbol{R}, z, \boldsymbol{u}) - \langle\langle V(\boldsymbol{R}, z, \boldsymbol{u})\rangle\rangle,$$

where the symbol $\langle\langle \cdots \rangle\rangle$ denotes a thermal average over the phonon field. The solution of the scattering problem is given by the set of eqs. (2.29)–(2.32). However, as the system studied is composed of the crystal and the scattered particle, the Green operator is a function of the total energy and Hamiltonian of this system, i.e.,

$$\tilde{G}^+ = \left(\tilde{E}_i^{\mathrm{p}} + \tilde{E}_i^{\mathrm{c}} - \tilde{H}_0 - \tilde{H}_{\mathrm{c}} + \mathrm{i}\epsilon\right)^{-1}, \tag{5.1}$$

with $H_0 = -(\hbar^2/2m)\Delta + U(z)$, and H_{c} the crystal Hamiltonian. E_i^{p} and E_i^{c} are respectively the energy of the particle and the crystal in the incident conditions. The sum of these two quantities will be conserved in the scattering process.

As v_1 does not depend upon the phonon operator $\boldsymbol{u}$, the matrix elements h describe a pure elastic scattering by a potential which has again the periodicity of the primitive lattice. The process is one of diffraction and the corresponding intensities are distributed among the different open diffraction channels. The t matrix elements and consequently the s ones exhibit the exchange of energy between particle and crystal by the exchange of real or virtual phonons. To go further, expression (2.11) giving the transition rate is transformed using the Van Hove [21] procedure and one gets:

$${}_f w_i = \hbar^{-2} \int_{-\infty}^{+\infty} \exp\left[\mathrm{i}\frac{\lambda}{\hbar}\left(E_f^{\mathrm{p}} - E_i^{\mathrm{p}}\right)\right] \langle\langle {}_i T_f^+(0)\ {}_f T_i(\lambda)\rangle\rangle \, \mathrm{d}\lambda, \tag{5.2}$$

where E_f^{p} and E_i^{p} are respectively the final and initial energies of the particle and ${}_f T_i$ the total matrix element calculated between final and initial states. Due to the thermal average operation noted by $\langle\langle \cdots \rangle\rangle$, the crystal states disappear. However, the product of T matrix elements in the double bracket exhibits correlation functions of the $\boldsymbol{u}$ operator for two different values of λ, a parameter which has the dimension of time.

Now writing eq. (2.31) in a condensed manner

$$T = h + L, \tag{5.3}$$

where L contains all the inelastic process, the averaged factor in eq. (5.2) becomes

$$\left|{}_f h_i + \langle\langle {}_f L_i(\lambda)\rangle\rangle\right|^2 + \left(\langle\langle {}_i L_f^+(0)\ {}_f L_i(\lambda)\rangle\rangle - \left|\langle\langle {}_f L_i(\lambda)\rangle\rangle\right|^2\right). \tag{5.4}$$

As $\langle\langle {}_f L_i(\lambda)\rangle\rangle$ does not contain correlation function for two different λ values, the integration over λ with the first term of eq. (5.4) yields a δ function. One gets:

$$\begin{aligned} {}_f w_i = {} & \frac{2\pi}{\hbar}\delta\left(E_f^{\mathrm{p}} - E_i^{\mathrm{p}}\right)\left|{}_f h_i + \langle\langle {}_f L_i(\lambda)\rangle\rangle\right|^2 \\ & + \hbar^{-2}\int_{-\infty}^{+\infty} \exp\left(\mathrm{i}\frac{\lambda}{\hbar}\left(E_f^{\mathrm{p}} - E_i^{\mathrm{p}}\right)\right)\left(\langle\langle {}_i L_f^+(0)\ {}_f L_i(\lambda)\rangle\rangle - \left|\langle\langle {}_f L_i(\lambda)\rangle\rangle\right|^2\right) \mathrm{d}\lambda. \end{aligned} \tag{5.5}$$

Then the transition rate is composed of two terms giving, respectively, the rates for the elastic and the inelastic processes.

In order to simplify the subsequent analysis and the numerical calculation we consider a particle scattered by a dense surface, like the (111) or (100) faces of metals, for which the diffraction peak intensities are very small. In this case the h values are small and can be neglected in the L expression. Then one has $L = s = t$ and the reflection coefficient is given by

$$
{}_fR_i = \frac{2\pi^2}{p_i}\delta\left(\tilde{E}_f^{\mathrm{p}} - \tilde{E}_i^{\mathrm{p}}\right)\left|{}_f\tilde{h}_i + \left\langle\left\langle {}_f\tilde{t}_i(\alpha)\right\rangle\right\rangle\right|^2
$$
$$
+ \frac{\pi}{p_i}\int_{-\infty}^{+\infty}\exp\left(\mathrm{i}\alpha\left(\tilde{E}_f^{\mathrm{p}} - \tilde{E}_i^{\mathrm{p}}\right)\right)\left(\left\langle\left\langle {}_i\tilde{t}_f^{+}(0)\ {}_f\tilde{t}_i(\alpha)\right\rangle\right\rangle - \left|\left\langle\left\langle {}_f\tilde{t}_i(\alpha)\right\rangle\right\rangle\right|^2\right)\mathrm{d}\alpha. \tag{5.6}
$$

5.2. Coherent intensities

It is necessary, in order to obtain these quantities, to calculate the averaged matrix element $\langle\langle \cdots \rangle\rangle$ included in the first term of eq. (5.6). The averaged t matrix is the solution of the following equation:

$$
\langle\langle t\rangle\rangle = \langle\langle v_2\rangle\rangle + \langle\langle v_2 G^{+} t\rangle\rangle. \tag{5.7}
$$

In order to perform the average of the last term, we start with the Green operator (5.1) expressed in an integral form [22,23] with dimensionless quantities, i.e.,

$$
\tilde{G}^{+} = -\mathrm{i}\int_0^{\infty}\exp\left[\mathrm{i}\alpha\left(\tilde{E}_i^{\mathrm{p}} + \tilde{E}_i^{\mathrm{c}} - \tilde{H}_0 - \tilde{H}_c + \mathrm{i}\epsilon\right)\right]\mathrm{d}\alpha. \tag{5.8}
$$

Then introducing this expression in eq. (5.7), it is easy to show that:

$$
\langle\langle \tilde{t}\rangle\rangle = \langle\langle \tilde{v}_2\rangle\rangle - \mathrm{i}\int_{-\infty}^{+\infty}\mathrm{d}\alpha\left\langle\left\langle \tilde{v}_i(\boldsymbol{R}, z, u(\alpha))\ \tilde{G}_i^{+}(\alpha)\tilde{t}\right\rangle\right\rangle, \tag{5.9}
$$

where:

(i) $G_i^{+}(\alpha) = \exp[\mathrm{i}\alpha(\tilde{E}_i^{\mathrm{p}} - \tilde{H}_0 + \mathrm{i}\epsilon)]$, depends only on the particle coordinates;

(ii) $\tilde{v}_i(\boldsymbol{R}, z, \alpha) = \exp(\mathrm{i}\alpha\tilde{H}_{\mathrm{c}})\ \tilde{v}_2(\boldsymbol{R}, z, \boldsymbol{u})\ \exp(-\mathrm{i}\alpha\tilde{H}_{\mathrm{c}})$, is the potential v_2 in the interaction picture.

Now we proceed to the iteration of the t matrix equation. In general form it is written as

$$
t = \underset{1}{v_2} + \underset{2}{v_2 G^{+} v_2} + \underset{3}{v_2 G^{+} v_2 G^{+} v_2} + \underset{\cdots}{\cdots}, \tag{5.10}
$$

where the number under each term labels the expansion or perturbation order. Noting that $\langle\langle \tilde{v}_2\rangle\rangle = 0$, and taking the matrix element $\langle\Phi_i| \cdots |\Phi_i\rangle$ of each term, eq. (5.9) is expanded into

$$
\left\langle\left\langle {}_i\tilde{t}_i\right\rangle\right\rangle = -\mathrm{i}\int_{-\infty}^{+\infty}\mathrm{d}\alpha\left\langle\Phi_i\right|\left\langle\left\langle \tilde{v}_i(\alpha)\ \tilde{G}_i^{+}(\alpha)\ \tilde{v}_i(0)\right\rangle\right\rangle\left|\Phi_i\right\rangle
$$
$$
+ (-i)^2\int_{-\infty}^{+\infty}\mathrm{d}\alpha_2\int_{-\infty}^{+\infty}\mathrm{d}\alpha_1\left\langle\Phi_i\right|\left\langle\left\langle \tilde{v}_i(\alpha_1+\alpha_2)\ \tilde{G}_i^{+}(\alpha_2)\ \tilde{v}_i(\alpha_1)\ \tilde{G}_i^{+}(\alpha_1)\ \tilde{v}_i(0)\right\rangle\right\rangle\left|\Phi_i\right\rangle + \cdots, \tag{5.11}
$$

an expression in which the thermal average can be performed knowing the explicit expression of $\tilde{v}_2$, as the Green operator does not depend upon the phonon operator $\boldsymbol{u}$. In this way the solution is given by the sum of the matrix elements $\langle\langle {}_i\tilde{t}_i^{(m)}\rangle\rangle$ at the various orders m of perturbation, i.e.,

$$
\left\langle\left\langle {}_i\tilde{t}_i\right\rangle\right\rangle = \sum_{m=2}^{\infty}\left\langle\left\langle {}_i\tilde{t}_i^{(m)}\right\rangle\right\rangle. \tag{5.12}
$$

5.2.1. Second-order perturbation

Let us examine the second-order term. The average $\langle\langle v_i[\boldsymbol{u}(\alpha)]\ v_i[\boldsymbol{u}(0)]\rangle\rangle$ yields a function of the correlated displacement $f(\langle\langle u(\alpha)\ u(0)\rangle\rangle)$ with [23,24]

$$\chi^2\langle\langle u(\alpha)\ u(0)\rangle\rangle = \frac{m}{M}\int_{-\Omega_{\max}}^{+\Omega_{\max}} \frac{\rho(\Omega)}{\Omega} n(\Omega)\ \exp(\mathrm{i}\alpha\Omega)\ \mathrm{d}\Omega, \tag{5.13}$$

an expression in which $\rho(\Omega)$ is the spectral density for the dimensionless phonon frequency Ω ($\Omega = A^2\hbar\omega$), $n(\Omega)$ is the Bose–Einstein factor and M the mass of a crystal atom.

To go further one expands the (analytical) function f in powers of the correlated displacement u. The general term, $(\langle\langle u(\alpha)\ u(0)\rangle\rangle)^n$ is proportional to $\exp(\mathrm{i}\alpha\Sigma_{q=1}^{n}\Omega_q)$ and the subsequent integration over α yields a dressed Green operator:

$$\tilde{G}_i^+(\alpha) \to (G^+)^{-1} = \tilde{E}_i^{\mathrm{p}} - \tilde{H}_0 + \sum_{q=1}^{n}\Omega_q + \mathrm{i}\epsilon. \tag{5.14}$$

There remain n integrations over the different Ω_q variables, corresponding to an exchange of n phonons. The result will be proportional to T^n at sufficiently high crystal temperature T. The calculation is achieved by introducing the projector of Φ states. As the dressed Green operator is located between two matrix elements the exchange of phonons is virtual, i.e., the particle is first scattered by the potential (matrix element) where it exchanges some phonons, then propagates in this intermediate state, which does not necessarily conserve energy, and finally is scattered again by the potential with the reverse exchange of phonons. On the whole, the energy of the particle is conserved. With this calculation procedure the matrix element $\langle\langle_i \tilde{t}_i^{(2)}\rangle\rangle$ is decomposed into a sum of submatrix elements $\langle\langle_i \tilde{t}_i^{(2,n)}\rangle\rangle$, each one depicting the virtual exchange of n phonons, i.e.,

$$\left\langle\left\langle_i \tilde{t}_i^{(2)}\right\rangle\right\rangle = \sum_{n=1}^{\infty}\left\langle\left\langle_i \tilde{t}_i^{(2,n)}\right\rangle\right\rangle. \tag{5.15}$$

5.2.2. Higher-order perturbation

The same analysis can be done for the third-order term. But due to the presence of the potential in between the products $\tilde{v}_i\tilde{G}_i^+$ and $\tilde{G}_i^+\tilde{v}_i$, the process can include also the virtual exchange of two successive phonons. The complete analysis has been carried out in previous publications [23,24]. Let us outline here that, at this order, the matrix element $\langle\langle_i \tilde{t}_i^{(3)}\rangle\rangle$ does not exhibit the single virtual phonon process. Therefore it is given by

$$\left\langle\left\langle_i \tilde{t}_i^{(3)}\right\rangle\right\rangle = \sum_{n=2}^{\infty}\left\langle\left\langle_i \tilde{t}_i^{(3,n)}\right\rangle\right\rangle. \tag{5.16}$$

Going further in the order expansion, previous analysis [25] has shown that

$$\left\langle\left\langle_i \tilde{t}_i^{(m)}\right\rangle\right\rangle = \sum_{n=n_m}^{\infty}\left\langle\left\langle_i \tilde{t}_i^{(m,n)}\right\rangle\right\rangle, \tag{5.17}$$

with n_m equal to $m/2$ and $(m+1)/2$ for m even or odd, respectively. In fig. 3, all the one and two virtual phonon processes for orders of m equal to two through four have been represented by a diagram. Here, as usual, a point represents a matrix element of the potential and a pair of straight and curved lines a dressed Green operator. One sees that the matrix elements such as $\langle\langle_i \tilde{t}_i^{(3,2)}\rangle\rangle$ or $\langle\langle_i \tilde{t}_i^{(4,2)}\rangle\rangle$ are composed of three different contributions. For each of them there corresponds a unique expression to be

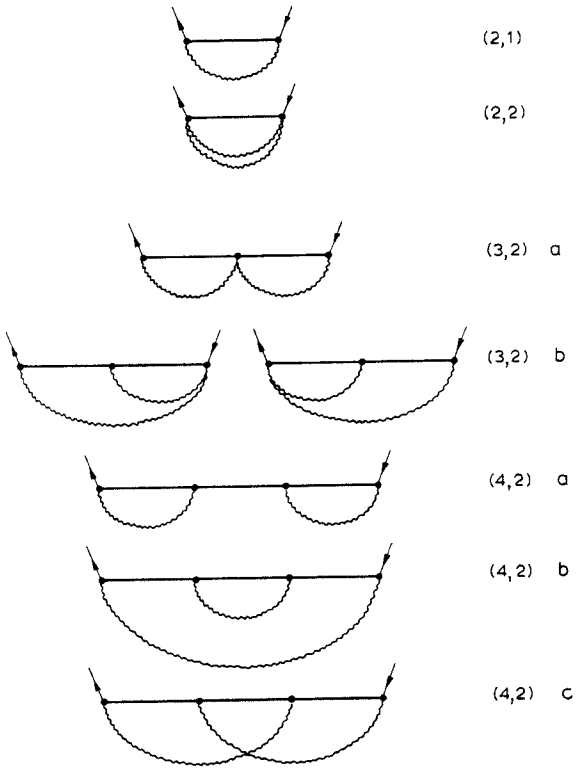

Fig. 3. Elastic diagram for one and two virtual phonon exchanges.

calculated. The number of contributions or diagrams for given m and n integers, increases rapidly with m or n. These numbers have been calculated previously [25] where the (4,3), (5,3), and (6,3) diagrams are presented.

5.3. Inelastic intensities

These intensities are given by the second term of eq. (5.6). Replacing t by the expansion of eq. (5.10), the bracket under the integration is written as

$$\left\langle\left\langle {}_i\tilde{t}_f^{+}(0)\ {}_f\tilde{t}_i(\alpha)\right\rangle\right\rangle - \left|\left\langle\left\langle {}_f\tilde{t}_i\right\rangle\right\rangle\right|^2 = \left\langle\left\langle {}_i(\tilde{v}_i^{+}(0))_{ff}(\tilde{v}_i(\alpha))_i\right\rangle\right\rangle + \left\langle\left\langle {}_i(\tilde{v}_i^{+}(0))_{ff}\left(\tilde{v}_i(\alpha)\ \tilde{G}^{+}\tilde{v}_i(\alpha)\right)_i\right\rangle\right\rangle$$
$$- \left|\left\langle\left\langle {}_f(\tilde{v}_i)_i\right\rangle\right\rangle + \left\langle\left\langle {}_f\left(\tilde{v}_i\tilde{G}^{+}\tilde{v}_i\right)_i\right\rangle\right\rangle + \cdots\right|^2, \tag{5.18}$$

or in a shorthand form, which uses an integer in place of the perturbation order term:

$$\left\langle\left\langle {}_i\tilde{t}_f^{+}(0)\ {}_f\tilde{t}_i(\alpha)\right\rangle\right\rangle - \left|\left\langle\left\langle {}_f\tilde{t}_i\right\rangle\right\rangle\right|^2 = \langle\langle 1^{+}\ 1\rangle\rangle + \langle\langle 1^{+}\ 2\rangle\rangle + \langle\langle 2^{+}\ 1\rangle\rangle + \langle\langle 1^{+}\ 3\rangle\rangle + \langle\langle 3^{+}\ 1\rangle\rangle + \langle\langle 2^{+}\ 2\rangle\rangle$$
$$+ \cdots - |\langle\langle 2\rangle\rangle + \langle\langle 3\rangle\rangle + \cdots|^2. \tag{5.19}$$

Generally speaking, with m representing the perturbation term of order m, to a term $\langle\langle m^{+}\ m'\rangle\rangle$ one can associate its conjugate $\langle\langle m'^{+}\ m\rangle\rangle$, except obviously for $m = m'$. As indicated by eq. (5.19), the short

hand notation m represents a matrix element taken between initial (i) and final (f) states of an operator equal to the product of $m\tilde{v}_i$ potential and $m-1$ Green operators, i.e.,

$$ {}_fm_i(\alpha) = \langle \Phi_f | \tilde{v}_i(\alpha)\ \tilde{G}^+ \tilde{v}_i(\alpha) \cdots \tilde{v}_i(\alpha)\ \tilde{G}^+\ \tilde{v}_i(\alpha) | \Phi \rangle, \tag{5.20} $$

$$ {}_im_f^+(0) = \langle \Phi_i | \tilde{v}_i(0)\ \tilde{G}^-\ \tilde{v}_i(0) \cdots \tilde{v}_i(0)\ \tilde{G}^-\ \tilde{v}_i(0) | \Phi_f \rangle, \tag{5.21} $$

equations in which $\tilde{v}_2$ and therefore $\tilde{v}_i$ is assumed to be real and Φ, as mentioned above in eq. (2.13), is an eigenstate of H_0. Therefore ${}_im_f^-$ is equal to

$$ {}_im_f^+(0) = \langle \Phi_f | \tilde{v}_i(0)\ \tilde{G}^-\tilde{v}_i(0) \cdots \tilde{v}_i(0)\ \tilde{G}^+\ \tilde{v}_i(0) | \Phi_i \rangle^* = {}_fm_i(0)^*, \tag{5.22} $$

i.e., the complex conjugate of ${}_fm_i(0)$. The sum of the two associated terms becomes

$$ \langle\langle {}_im_f^+\ {}_fm_i' \rangle\rangle + \langle\langle {}_im_f'^+\ {}_fm_i \rangle\rangle = 2\ \mathrm{Re}\big(\langle\langle {}_fm_i'(0)^*\ {}_fm_i(\alpha) \rangle\rangle\big) \tag{5.23} $$

and

$$ \langle\langle {}_i\tilde{t}_f^+(0)\ {}_f\tilde{t}_i(\alpha) \rangle\rangle - |\langle\langle {}_f\tilde{t}_i \rangle\rangle|^2 = \sum_1^\infty \big(\langle\langle {}_fm_i(0)^*\ {}_fm_i(\alpha) \rangle\rangle - |\langle\langle {}_fm_i \rangle\rangle|^2\big) $$
$$ - 2\ \mathrm{Re} \sum_{m'=1}^{\infty} \sum_{m=1}^{m'-1} \langle\langle {}_fm_i'(0)^*\ {}_fm_i(\alpha) \rangle\rangle. \tag{5.24} $$

5.3.1. First-order perturbation

As previously done for the calculation of the coherent intensity, we examine in detail the first term namely the $\langle\langle 1^+\ 1 \rangle\rangle$. Its contribution to the reflection coefficient is given by

$$ {}_fR_i^{(1^+1)} = \frac{\pi}{p_i} \int_{-\infty}^{+\infty} \exp\big[i\alpha\big(\tilde{E}_f^{\mathrm{p}} - \tilde{E}_i^{\mathrm{p}}\big)\big]\ \big\langle\big\langle \langle \Phi_i | \tilde{v}_i(0) | \Phi_f \rangle \langle \Phi_f | \tilde{v}_i(\alpha) | \Phi_i \rangle \big\rangle\big\rangle\ \mathrm{d}\alpha. \tag{5.25} $$

The thermal average of the product of the two potentials yields the same function f of the correlated displacement as those encountered in the calculation of the coherent $\langle\langle {}_i\tilde{t}_i^{(2)} \rangle\rangle$ term. As we have proceeded in analysing this expression, the function f is expanded in powers of $\langle\langle u(0)\ u(\alpha) \rangle\rangle$. The general term is proportional to $\exp[-\alpha \sum_{q=1}^{n} \Omega_q]$ and subsequent integration over α yields:

$$ 2\pi\delta\left(\tilde{E}_f^{\mathrm{p}} - \tilde{E}_i^{\mathrm{p}} - \sum_{q=1}^{n} \Omega_q\right). \tag{5.26} $$

In the remaining integrations over the n variables Ω_q, this delta function yields an exchange of n real phonons and, in the final state, the particle has exchanged with the crystal the phonon energy. The corresponding contribution to the reflection coefficient will be proportional to T^n and its magnitude depends upon the values of the potential matrix elements. Therefore the expansion of the f function leads one to express the reflection coefficient of the first-order perturbation by a sum of terms, each of them depicting the exchange of a given number n of real phonons, i.e.,

$$ {}_fR_i^{(1^+1)} = \sum_{n=1}^{\infty} {}_fR_i^{(1^+1,n)}. \tag{5.27} $$

The above analysis of the coherent matrix element $\langle\langle {}_i\tilde{t}_i^{(2)} \rangle\rangle$ and of the inelastic reflection coefficient

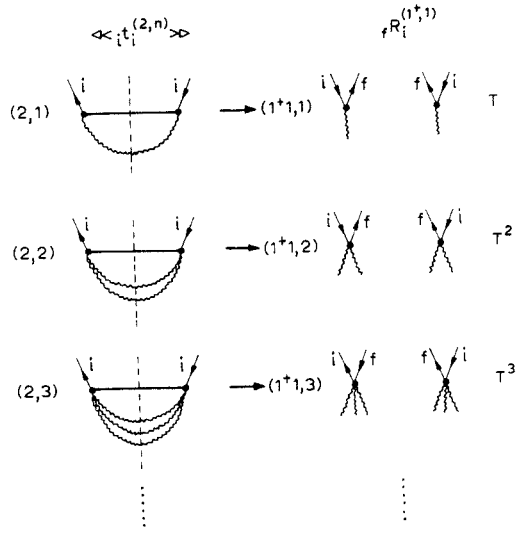

Fig. 4. Procedure for obtaining the inelastic reflection coefficient diagrams (right-hand side) from elastic diagrams (left-hand side). The vertical dashed line is the cutting line. The ${}_fR_i$ diagram labeled $(1^+1, 1)$ is the DWBA term. The last column gives the proportionality to the power of crystal temperature T (for T sufficiently high such that $\langle\langle N(\Omega)\rangle\rangle \sim T$).

${}_fR_i^{(1^+1)}$, which are very similar, suggests a close correspondence between them. Effectively one can demonstrate that [20]:

(i) Knowing the detailed expression of $\langle\langle {}_i\tilde{t}_i^{(2,n)}\rangle\rangle$, one can deduce without any calculation the corresponding ${}_fR_i^{(1^+1,n)}$ expression, by applying the following rules:
- Take the on-energy-shell part of the dressed propagator. This is equivalent to replacing the dressed propagator by a δ function containing the phonons involved in the propagator.
- Replace the projection on all states by projection on the final state.
- Multiply by $2\pi^2/p_i$.

On the diagrams which represent the $\langle\langle {}_i\tilde{t}_i^{(2,n)}\rangle\rangle$ matrix elements, these rules are equivalent to cutting the dressed propagator between two vertices as shown in fig. 4. The two coupled diagrams thus obtained represent a reflection coefficient denoted $(1^+\ 1,\ n)$, where n is the number of real phonons exchanged. At this order of perturbation n can take all integer values.

(ii) Knowing the $\langle\langle {}_i\tilde{t}_i^{(2)}\rangle\rangle$ value, which allows one to calculate the specular intensity at first order, one can obtain the total inelastic reflection coefficient for this order. Effectively one demonstrates [20] a form of the unitarity relation, which appears as

$$-\frac{2\pi}{p_i}\mathrm{Im}\left\langle\left\langle {}_i\tilde{t}_i^{(2)}\right\rangle\right\rangle = \sum_f {}_fR_i^{(1^+1)} = \left(\sum_f {}_fR_i^{(1^+1)}\right)_c + \left(\sum_f {}_fR_i^{(1^+1)}\right)_b, \tag{5.28}$$

where the sum is extended over all final states and can be decomposed into the contribution on continuum (c) and bound (b) states. As in the calculation of $\langle\langle {}_i\tilde{t}_i^{(2)}\rangle\rangle$ we use just one projector, this matrix element can be also decomposed into contributions of c and b states. One deduces easily that

$$-\frac{2\pi}{p_i}\left\{\mathrm{Im}\left\langle\left\langle {}_i\tilde{t}_i^{(2)}\right\rangle\right\rangle_{c+b} - \mathrm{Im}\left\langle\left\langle {}_i\tilde{t}_i^{(2)}\right\rangle\right\rangle_c\right\} = \left(\sum_f {}_fR_i^{(1^+1)}\right)_b. \tag{5.29}$$

Note that the right hand side of this expression is equal to the sticking coefficient (see section 8 below)

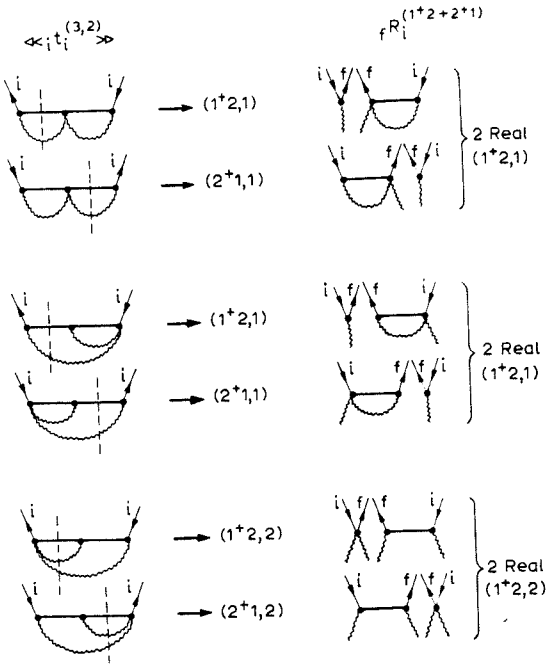

Fig. 5. Inelastic reflection coefficient diagrams obtained with the three elastic diagrams (3,2) with the procedure used in fig. 4. Cutting a propagator located on the right of the middle vertex yields a diagaram with time reversed.

corresponding to the $\langle\langle 1^+\ 1\rangle\rangle$ inelastic process. Therefore this quantity can be directly obtained from the $\langle\langle {}_i\tilde{t}_i^{(2)}\rangle\rangle$ value.

5.3.2. Second-order perturbation

The next term in ascending order of perturbation is the $\langle\langle 1^+\ 2\rangle\rangle + \langle\langle 2^+\ 1\rangle\rangle$. The first one is

$$\left\langle\left\langle\left\langle \Phi_i\right|\tilde{v}_i(0)\left|\Phi_f\right\rangle\left\langle\Phi_f\right|\tilde{v}_i(\alpha)\ \tilde{G}^+\ \tilde{v}_i(\alpha)\left|\Phi_i\right\rangle\right\rangle\right\rangle. \tag{5.30}$$

The preceding analysis can be done in the same way as for first-order term. It shows that the presence of a Green operator between two v_i potentials yields the appearance of virtual phonon processes which couple to the exchange of real phonons. Moreover the comparison to the following expression

$$\left\langle\left\langle\left\langle \Phi_i\right|\tilde{v}_i\tilde{G}^+\tilde{v}_i\tilde{G}^+\tilde{v}_i\left|\Phi_i\right\rangle\right\rangle\right\rangle \tag{5.31}$$

involved in the calculation of the coherent matrix element $\langle\langle {}_i t_i^{(3)}\rangle\rangle$, allows one to demonstrate [20] that the rules established for the first-order case are valid also. Hence, knowing the matrix elements or diagrams one deduces uniquely the corresponding expressions or diagrams for the inelastic reflection coefficients. As the first term in the sum (5.16), $\langle\langle {}_i t_i^{(3,2)}\rangle\rangle$ involve a two virtual phonon process, the first ${}_fR_i$ coefficient at this order contains an exchange of one real and one virtual phonon. It is then proportional to T^2. Consequently, the only component of ${}_fR_i$ proportional to T is given by the term $(1^+\ 1,\ 1)$ in fig. 4 which is the well known distorted wave Born approximation. Figure 5 depicts the different inelastic diagrams deduced from the $\langle\langle {}_i t_i^{(3,2)}\rangle\rangle$ coherent matrix elements.

The above analysis can be extended to higher-order terms. In this way one demonstrates [20] the validity for any order of the rules of correspondence, established here only for the first-order case. This

allows one to work with diagrams, and knowing the coherent expressions, to deduce the corresponding inelastic ones.

6. Thermal attenuation of the specular intensity

6.1. Potential

The above analysis is quite general and consequently the calculation procedure exposed above can be applied to any kind of potential. From subsection 5.2 we restrict ourselves to the case of particles scattered by a flat surface. If this is not the case, the diffraction process should be introduced in the calculation of the L matrix elements which are not equal to the t ones, (eq. (5.5)). Then the procedure starting with an integral representation of the Green operator allows one to decompose the reflection coefficients into a sum of virtual phonons processes. However, in order to simplify the calculation, and also to get insight into the physical phenomena, we consider, as indicated above, the scattering of a particle by a dense face of a metal, namely the (100) face of an fcc crystal. Then the particle surface interaction can be modeled by a soft potential, namely

$$V = D\left[\exp(-2\chi(z-u) - 2\chi^2\langle\langle u^2\rangle\rangle) - f_a(z)\right]. \tag{6.1}$$

Its repulsive part is thermally displaced in the direction normal to the surface through the displacement operator $\boldsymbol{u}$, and the attractive one is stationary with respect to thermal fluctuation. The displacement operator $\boldsymbol{u}$ should be suitably chosen in order to reproduce, as closely as possible the influence of crystal atom motion on the potential. There is no theoretical calculation of this influence. However, one knows that the potential is to a first approximation, proportional to the surface electronic density. Then the thermal displacement of the repulsive part of the potential is directly a consequence of the thermal electronic fluctuations, themselves linked to the motion of the atoms located close to the point where the potential is evaluated. To take account of this collective effect, we have proposed to model it by taking the displacement u equal to the mean displacement of the four atoms belonging to the (100) unit cell [22,26]. A simple calculation shows that the spectral density which enters into the calculation of the correlated displacements eq. (5.13) is equal to

$$\rho(\Omega) = \tfrac{1}{4}{}^z\rho_1^z + \tfrac{1}{2}{}^z\rho_2^z + \tfrac{1}{4}{}^z\rho_3^z, \tag{6.2}$$

where the subscripts 11, 12 and 13 label respectively the spectral density for an atom on itself, the correlated spectral density between nearest and next nearest neighbours. These quantities are given by the imaginary part of the Green functions of surface atoms and have been calculated exactly in a previous work [27]. The superscripts z labels the direction normal to the surface. The potential v_2 is easily calculated. One gets

$$v_2 = D\,\exp(-2\chi z)\left[\exp(2\chi u - 2\chi^2\langle\langle u^2\rangle\rangle) - 1\right], \tag{6.3}$$

a quantity which is independent of the shape of the attractive potential part f_a. Hence, its influence on the exchange of real or virtual phonons will certainly be weak compared to the influence of parameters contained in v_2. So we chose for this function a convenient shape namely $2\exp(-\chi z)$. Taking $v_1 = 0$, the distorted potential $U(z)$ in the Hamiltonian H_0 is of Morse shape, a potential for which the analytical form of bound state energies and matrix elements are known. Now the determination of the equipotential of V [24] indicates that the potential thermal displacement is equal to $2u$ for $V = 0$ and u for very large values of V/D. In the experiments, the energy of the incident particle is at most ten time the well depth, corresponding to a thermal displacement of the potential of the order of $2u$. In order to recover

the correct value u, this quantity should be divided by 2, an operation which is done by multiplying the spectral density by $\frac{1}{4}$ in the numerical calculations.

For such a choice of model potential, the particle can lose or gain energy without any change of its momentum component parallel to the surface. Hence, the description of physical reality is not complete. However, one can expect to get a correct description of the inelastic scattering phenomena and the correct influence of the different parameters.

6.2. Second-order perturbation

As explained above the $\langle\langle {}_i\tilde{t}_i^{(2)}\rangle\rangle$ term is a sum of contributions, each of them involving the exchange of a given number of virtual phonons, eq. (5.15), resulting from the expansion of the function f (section 5.2.1). With the chosen potential this function is

$$\exp\left(4\chi^2\langle\langle u(\alpha)\, u(0)\rangle\rangle\right) - 1 \tag{6.4}$$

and the contribution of n virtual phonons is given by

$$\left\langle\left\langle {}_i\tilde{t}_i^{(2,n)}\right\rangle\right\rangle = (A^2D)\frac{1}{n!}\left(\frac{4m}{M}\right)^n\left(\int_0^\infty {}_{p_i}l_p\, G^{(2,n)}(c_p)\, {}_pl_{p_i}\, \mathrm{d}p + \sum_b {}_{p_i}l_b\, G^{(2,n)}(c_b)\, {}_bl_{p_i}\right), \tag{6.5}$$

where $c_p = p_i^2 - p^2$, $c_b = p_i^2 + \Omega_b$, ${}_{p,b}l_{q,b'} = \langle\phi_{p,b}|\exp(-2\chi z)|\phi_{q,b'}\rangle$, and

$$G^{(2,n)}(c_{p,b}) = \int_{-\Omega_{\max}}^{+\Omega_{\max}}\cdots\int_{-\Omega_{\max}}^{+\Omega_{\max}}\frac{1}{c_{p,b} + \sum_{q=1,n}\Omega_q + \mathrm{i}\epsilon}\prod_{q=1}^{n}\frac{\rho(\Omega_q)}{\Omega_q}\left\langle\left\langle n(\Omega_q)\right\rangle\right\rangle \mathrm{d}\Omega_q. \tag{6.6}$$

The repeated integration over Ω yields an auto convolution of the function $\rho(\Omega)$. Therefore, one can expect that its shape does not affect the final result for a large n value. However, due to the factor $(1/n!)(4m/M)^n$ the corresponding matrix element will be negligible if the ratio m/M is not too large. This is the case for a helium atom scattered by a copper crystal, where calculations show that the terms corresponding to $n \geq 3$ are completely negligible.

6.3. Third-order perturbation

The matrix element corresponding to the diagram (3,2) in fig. 3 can be written directly following the diagram prescriptions. It is composed of three l matrix separated by $G^{(2,1)}$ functions

$$\left\langle\left\langle {}_i\tilde{t}_i^{(3,2)}\right\rangle\right\rangle = (A^2D)\left(\frac{4m}{M}\right)^2\left(\int_0^\infty\int_0^\infty {}_{p_i}l_q\, G^{(2,1)}(c_q)\, {}_ql_p\, G^{(2,1)}(c_p)\, {}_pl_{p_i}\, \mathrm{d}p\, \mathrm{d}q + \cdots\right), \tag{6.7}$$

where the $\cdots$ indicates that one should add three terms constructed with the intermediate state p or q, and p and q, replaced by bound states. The integrations are then replaced by a summation over all the bound states. In the same way, the matrix element of the diagram (3,2) b can be written. One gets

$$\left\langle\left\langle {}_i\tilde{t}_i^{(3,2)}\right\rangle\right\rangle = (A^2D)\left(\frac{4m}{M}\right)^2\left[\int_0^\infty\int_0^\infty {}_{pi}l_p\, {}_pl_q\left(G^{(3,2)}(c_q, c_p) + G^{(3,2)}(c_p, c_q)\right){}_ql_{p_i}\, \mathrm{d}p\, \mathrm{d}q + \cdots\right], \tag{6.8}$$

where the symbol $+\cdots$ has the same meaning as above and

$$G^{(3,2)}(c_p, c_q) = \int\int_{-\Omega_{max}}^{+\Omega_{max}} \frac{d\Omega_1}{c_p + \Omega_1 + i\epsilon} \frac{d\Omega_2}{c_q + \Omega_1 + \Omega_2 + i\epsilon} \prod_{r=1}^{2} \frac{\rho(\Omega_r)}{\Omega_r} \langle\langle n(\Omega_r)\rangle\rangle. \tag{6.9}$$

6.4. Fourth-order perturbation

There are three diagrams (4, 2) represented in fig. 3. The corresponding matrix elements are similar to that of eq. (6.8) but with three integrations. Also, the sum of two $G^{(3,2)}$ functions is replaced by one function $G^{(4,2)}$, each one being specific to the diagram considered. They contain the product of three dressed propagators and can be expressed as a function of $G^{(2,1)}$ for the first diagram and $G^{(3,2)}$ for the others [24].

6.5. Resummation procedure

One can show [25] that in any diagram, representing a virtual phonon exchange, there is no vertex which is not connected to a phonon line. This is a consequence of our choice of v_2 such that $\langle\langle v_2\rangle\rangle = 0$. This rule is equivalent to saying that there are never two successive free propagators $G_e^+ = (c_{p,b} + i\epsilon)^{-1}$. Then one can draw recursively the different diagrams corresponding to a process of order m involving an exchange of n virtual phonons. However, the nuber of diagrams increases very rapidly with m or n values. So it becomes necessary to find a calculation procedure for the sum of the $\langle\langle_i \bar{t}_i^{(m,n)}\rangle\rangle$ matrix elements starting with those which can be calculated easily, i.e., those listed in fig. 3. With this in mind let us define an operator g which has the effect of connecting two diagrams. For instance we have (2,1) g (2, 1) = (3, 2) a (fig. 3). Now one define a new T matrix T_R which is a solution of the equation

$$T_R = \Lambda + \Gamma(g + G_e^+)T_R. \tag{6.10}$$

The iteration of this equation gives a set of diagrams deduced from those contained in Λ and Γ by a direct touching connection (g) or by a connection through a free propagator. Λ and Γ are chosen in such a way that the set of diagrams generated is as large as possible while still avoiding duplications. These criteria lead one to take

$$\Lambda = (2, 1) + (2, 2) + (3, 2)\ \mathrm{b} + (4, 2)\ \mathrm{b} + (4, 2)\ \mathrm{c}, \tag{6.11}$$

$$\Gamma = (2, 1) + (2, 2) + X_3(\mathrm{it}) \times (3, 2)\ \mathrm{b} + X_4(\mathrm{it}) \times [(4, 2)\ \mathrm{b} + (4, 2)\ \mathrm{c}]. \tag{6.12}$$

However, this procedure does not generate the whole set of diagrams. In order to compensate this deficiency the diagrams (3, 2) b and the sum of (4, 2) b and (4, 2) c are multiplied by a number, respectively X_3(it) and X_4(it). These numbers vary from one iteration step to another (it) and are determined to take account of the values of the missing diagrams values [25]. Note that, if the first iteration contained the diagrams of Λ, the second one generates some of (3, 2) to (8, 4) type. Generally speaking the iteration step of order (it) introduces those of (it + 1, it) to (4it, 2it) type.

6.6. Results — an example

Numerical calculations have been performed for different incident particles, namely helium, molecular hydrogen and neon, particles which have at low kinetic energy a quantum behaviour. For each particle the potential parameters (D, χ) have been determined by interpretation of diffraction experiments. The remaining parameters are the experimental conditions, i.e., the incident angle and energy. In

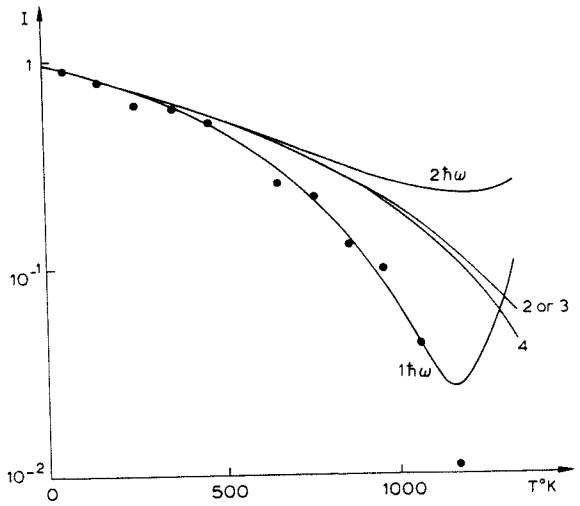

Fig. 6. Specular beam intensities for helium scattering from a Cu(100) face with incident energy 21 meV and incident angle of 55.5°. The curves labeled $1\hbar\omega$ and $2\hbar\omega$ are the intensitities given by the one-phonon and the one- plus two-phonon events, respectively. The resummed intensity curves are labeled by the iteration step number. Experimental data are from ref. [12].

any case the iteration process converges to stable intensity values for an iteration number larger than four, for all crystal temperatures T lower than the melting temperature. Figure 6 is an illustration of these results and depicts the attenuation of specular intensity with crystal temperature.

This attenuation differs from a usual Debye–Waller factor. Here the specular intensity decreases more rapidly than an exponential as the crystal temperature increases. The calculated intensities involving the one and one plus two virtual phonons exchange (curves labelled $1\hbar\omega$ and $2\hbar\omega$) have a minimum at $T \approx 1150$ K and after that they increase. This indicates clearly that in this temperature range these processes are not sufficient to describe the physical phenomena. In fact the successive iterations show that they give the correct intensity for temperature lower than 300 K.

Another general behaviour can be noticed. As the iteration number increases the intensities oscillate around their stable values. The $(1+2)\hbar\omega$ yields intensities larger than the $1\hbar\omega$ alone. Those yielded by the successive iterations are comprised between the two preceding ones. Moreover, the intensities yielded by iteration 2 are lower than those given by iteration 3, itself larger than those yielded by iteration 4. It seems that adding an even number of phonon events increases the intensities whereas adding an odd number yields the reverse effect. For helium scattering the resumed intensities, at iteration 4 for instance, are larger than the measured ones in the medium and high temperature range. The experimental data seems to be rather well represented by the $1\hbar\omega$ process. We do not think that this is due to the deficiency of our model [25], but it rather means that the amplitude of surface atom displacements are too small. The present calculation includes anharmonic effects through the quasi-harmonic approximation, but supposes that they are identical for surface and bulk atoms. One knows that near the surface the interaction potential between crystal atoms is different from that which prevails between bulk atoms. This leads one to consider that anharmonic effects could be increased in and near the surface plane. With this hypothesis, the mean square displacements of surface atoms have been calculated in order to recover the experimental data [28]. As this quantity becomes larger than the corresponding bulk ones above 500 K, this surface enhancement can be due to enhanced surface anharmonicity or, at higher temperature, to the beginning of thermal roughening. To our knowledge the respective contributions of these two phenomena, in the thermal attenuation of the specular beam, has not been clearly demonstrated.

6.7. Approximations

Having at our disposal a calculation procedure which yields a result close to the exact one, it is possible to test some approximations. This has been achieved in different ways [29,30]. But the best one [31], i.e., which allows one to recover the resummation results over a large domain of parameters, consists of summing the diagrams constructed with the one virtual phonon process separated by a free propagator:

$$\langle\langle {}_i\tilde{t}_i\rangle\rangle = (2,1) + (2,1)\, G_e^+\,(2,1) + (2,1)\, G_e^+\,(2,1)\, G_e^+(2,1) + \cdots . \tag{6.13}$$

Neglecting the principal value in the free propagator, the series to sum up is of geometric form and we get

$${}_iR_i = \left| \frac{1 - (i\pi/2p_i)\langle\langle {}_i\tilde{t}_i^{(2,1)}\rangle\rangle}{1 + (i\pi/2p_i)\langle\langle {}_i\tilde{t}_i^{(2,1)}\rangle\rangle} \right|^2 = \frac{(1-aT)^2 + bT^2}{(1+aT)^2 + bT^2}, \tag{6.14}$$

where a and b are constants with respect to the temperature T. This expression is a kind of Padé approximant. It is easy to calculate as it involves only the knowledge of the $\langle\langle {}_i\tilde{t}_i^{(2,1)}\rangle\rangle$ values.

7. Inelastic scattering

7.1. Expressions for the reflection coefficient

With the potential defined in section 6.1, the inelastic expressions involving the exchange of real phonons can be written with the help of the rules stated in section 3.1, applied to the elastic expressions or diagrams (2, n), (3, n), etc. This allows one to get the set of inelastic expressions. We limit ourselves to those which yield reflection coefficient proportional to T or T^2. In this way one enumerates the following:

(i) 1 real phonon term proportional to T, coming from the (2, 1, 1) elastic diagram (fig. 4),

(ii) 2 and 3 diagrams with one real and one virtual phonon exchange coming respectively from the (3, 2, 2) (fig. 5) and (4, 2, 2) elastic one. They yield a contribution proportional to T^2.

(iii) 4 diagrams with the exchange of two real phonons coming from the (2, 1, 2) fig. 4, (3, 2, 2) fig. 5 and (4, 2, 2) elastic contributions and also proportional to T^2.

Note that to other diagrams, there corresponds a contribution to the reflection coefficient proportional at least to T^3.

All the contributions listed from (i) to (iii) have been calculated and their analytical expressions published [20]. For clarity and conciseness we reproduce here some of them. Putting $\Omega_0 = A^2(E_f^p - E_i^p)$ the dimensionless particle exchange of energy, one has:

(i) For the one-phonon process proportional to T:

$${}_fR_i^{(1\,1,1)} = \frac{2\pi^2}{p_i}\left(\frac{4m}{M}\right)\frac{\rho(\Omega_0)}{\Omega_0}\langle\langle n(\Omega_0)\rangle\rangle({}_fl_i)^2. \tag{7.1}$$

This expression is the distorted wave Born approximation.

(ii) The first diagram of fig. 5 gives a contribution equal to

$${}_fR_i^{(1^+2,1)} = \frac{2\pi^2}{p_i}\left(\frac{4m}{M}\right)^2\frac{\rho(\Omega_0)}{\Omega_0}\langle\langle n(\Omega_0)\rangle\rangle_f l_i \times 2\,\mathrm{Re}\left(\int_0^\infty {}_fl_p\, G^{(2,1)}(c_p)\; {}_pl_i\, \mathrm{d}p + \sum_b {}_fl_b G^{(2,1)}(c_b)_b l_i\right), \tag{7.2}$$

in which $G^{(2,1)}$ is the dressed propagator eq. (6.6) accounting for the virtual phonon exchange. As there are on the whole two Bose–Einstein factors this quantity is proportional to T^2.

(iii) The last diagram of fig. 5 represents an exchange of two real phonons. The corresponding reflection coefficient is equal to

$$ {}_fR_i^{(1^+2,2)} = \frac{2\pi^2}{p_i}\left(\frac{4m}{M}\right)^2 {}_fl_i \; 2\,\mathrm{Re}\left[\int_0^\infty {}_fl_p \; G^{(2,1)}(c_p, \Omega_0)\; {}_pl_i \; \mathrm{d}p + \sum_b {}_fl_b \; G^{(2,1)}(c_b, \Omega_0)\; {}_bl_i\right], \tag{7.3} $$

with

$$ G^{(2,1)}(c_{p,b}, \Omega_0) = \int_{-\Omega_{\max}}^{+\Omega_{\max}} \frac{\rho(\Omega_0 - \Omega_1)}{\Omega_0 - \Omega_1} \langle\langle n(\Omega_0 - \Omega_1)\rangle\rangle \frac{\mathrm{d}\Omega_1}{c_{p,b} + \Omega_1 + \mathrm{i}\epsilon} \frac{\rho(\Omega_1)}{\Omega_1} \langle\langle n(\Omega_1)\rangle\rangle. \tag{7.4} $$

The particle exchanges the real phonon Ω_1 on the first vertex, then propagates with energy equal to $p_i^2 + \Omega_1$ and exchanges another real phonon on the second vertex.

7.2. *Results — an example*

As indicated above the elastic contributions corresponding to the diagrams of fig. 3 have been calculated. The inelastic reflection coefficients deduced from the elastic diagrams referred to above and listed in section 7.1 are now calculated and integrated over all the final states. The unitary relation (5.26) and those valid for higher order are verified. This leads one to think that there is no error in the numerical calculation, but one cannot be certain of this fact. Moreover, in order to satisfy the whole unitarity relation, the inelastic integrated value, say ${}_fR_i$, should be equal to $1 - I_{00}$, where I_{00} is the specular intensity calculated by the resummation procedure. The comparison between these quantities allows one to determine the domain of crystal temperature where the limited number of inelastic terms yields a correct result.

These considerations are illustrated in fig. 7. The curve labelled $(1)_t$ corresponds to ${}_fR_i$ values calculated with the distorted wave Born approximation term (7.1) to which has been added the contribution of the exchange of two real phonons $(1^+1, 2)$ of fig. 4. This last one yields a negligible contribution and the total values are proportional to T. The terms corresponding to diagrams of fig. 5 yield a small decrease of the ${}_fR_i$ values as indicated by the curve labelled $(1+2)_t$. Compared to the $1 - I_{00}$ values, one sees that the contribution of these term gives a correct result only for very low temperature. This domain of validity is extended up to approximately 300 K when one adds the contribution of the five inelastic diagrams deduced from the elastic (4, 2, 2) ones (curve labelled $(1+2+3)_t$). Moreover the ${}_fR_i$ values are strongly modified, the curve taking the shape of a parabola and exhibiting a maximum for $T \approx 800$ K. Going further, it is expected that terms proportional to T^3, which contain one, two and three real phonon events, act in such a way that the ${}_fR_i$ values increase in the region of the maximum and therefore extend the domain of validity of this partial calculation. For higher terms in powers of T, one expects to observe oscillation of the ${}_fR_i$ values in the same manner as those observed in the resummation procedure in the elastic calculation.

Figure 8 depicts the variation of the transition rate between the incident and a given final state, as a function of the crystal temperature. It includes the contribution of the ten diagrams listed above. The particle loses (a) or gains (b) energy. The curves labelled 1 and 2 give the transition rate, for events involving, respectively, the exchange of one and two real phonons. The latter is proportional to T^2 and the former is again a parabola shaped curve. The maximum, located about 300 K indicates the temperature range where the measurement of a one-phonon exchange will be the easiest. As above, one can expect that the introduction of terms proportional to T^3 will increase the transition rate in the

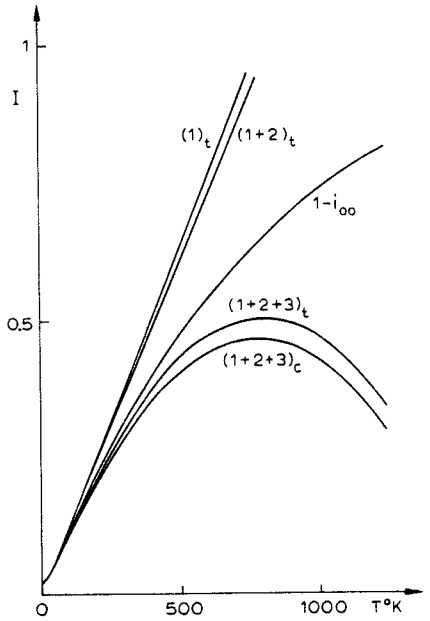

Fig. 7. Scattering of He by Cu(100) with incident energy 21 meV and incident angle 55.5°, which gives a normal energy of 6.74 meV. The curves labeled $(1)_t$, $(1+2)_t$, $(1+2+3)_t$, $1-I_{00}$ give the total inelastic transition probability calculated with unitarity relations for first order, first plus second order, first plus second plus third order, and to all orders, respectively. The curve labeled $(1+2+3)_c$ gives the total inelastic transition probability up to third order for the continuum states.

region of the maximum and above this point. Hence, this maximum could be shifted to higher temperatures. For the two phonon process their contribution will be certainly negative yielding the appearance of a maximum whereas the three-phonon transition rate will increase as T^3.

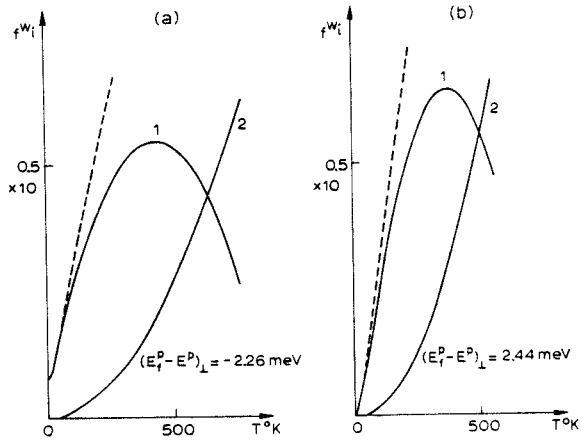

Fig. 8. Transition probability for He scattered by Cu(100) with incident energy 21 meV and incident angle 55.5°. (a) $\vartheta_f = 62.5°$, and (b) $\vartheta_f = 48.6°$. $E_f^p - E_i^p$ is the particle exchange of energy. The dashed line denotes the DWBA. The solid lines are calculated through 3rd order in perturbation theory including all terms in T and T^2. These curves labeled 1 and 2 give the one and two real phonon exchange, respectively.

8. Sticking

The inelastic formalism developed in the above sections allows for an immediate extension to the problem of sticking of atoms or molecules at surface. Sticking is an important and interesting problem, in part because it is the precursor process to many types of chemical reactions at surfaces. From a fundamental point of view, the simplest sticking processes are those involving the physisorption of small mass molecules and atoms, where quantum mechanical effects dominate, and this regime has recently received a substantial amount of experimental investigation [32,33].

If the gas molecules are massive, the theoretical treatment can be completely classical and the sticking is a straightforward process of energy loss upon collision or multiple collisions with the surface. For low mass and low energy particles which will become physisorbed to the surface (and not chemically bound) a quantum mechanical approach must be used and the description is not so simple. A very fundamental problem arises because the sticking problem is not a typical scattering process, in which the projectile begins and ends its trajectory in states far removed from the scattering center where the interaction potential is negligible. Classically, the problem is unambiguous. A particle residing near the surface with negative total translational energy is considered to be stuck, even if this state lasts only a short time. However, in the quantum regime, a particle near the surface, even if it is initially in a negative energy state, remains strongly under the influence of the interaction potential and continues to make transitions. Some of these subsequent transitions involve excursions to positive energy continuum states with non-zero probability that the particle leaves the surface region. For an isolated system, such transitions assure the fact that after a very long time, the probability of finding the particle near the surface will approach zero, i.e., for a isolated quantum mechanical system there is no sticking over infinitely long times. Thus for an isolated quantum mechanical system the definition of sticking is ambiguous at the very least. The theoretical definition of sticking must be operationally defined in order to match the manner in which the sticking coefficient is measured experimentally.

The simplest definition of quantum mechanical sticking, and the one we will use here, is the probability of transition into a negative energy bound state as calculated through various orders of perturbation theory. Thus the sticking coefficient σ_i is defined in terms of the transition rate of eq. (5.5) or the reflection coefficient (5.6) according to

$$\sigma_i = \sum_{b(E_\beta^b<0)} {}_bw_i/j_i = \sum_{b(E_\beta^b<0)} {}_bR_i, \tag{8.1}$$

where ${}_bw_i$ is calculated through several orders in perturbation theory. It should be noted in this context that diffraction can play a large role in the sticking process. In particular, the projectile can diffract into a bound state while keeping its total energy positive and this enhances the number of possible channels for subsequent energy loss to negative total energy. Under the special conditions of selective adsorption resonances, the projectile can undergo this diffraction process to a bound state while conserving its total translational energy, and this leads to markedly increased possibilities of inelastic exchange.

It is of interest to express the condition of unitarity, first shown in (2.25) and later expanded to the case of inelastic scattering in (5.28), in a form of interest to the sticking problem. This is

$$1 = \left\langle\!\!\left\langle \left| 1 \frac{i\pi}{p_i} {}_s\tilde{T}_i \right|^2 \right\rangle\!\!\right\rangle + \sum_{c\neq s} \pi^2 \frac{|{}_c\tilde{T}_i|^2}{p_i p_c} + \frac{2\pi}{p_i} \sum_b |{}_b\tilde{T}_i|^2. \tag{8.2}$$

This expression is valid at each order of perturbation theory. The three terms on the right-hand side are, respectively, the reflection coefficient into the specular beam, into inelastic continuum channels (and other elastic diffraction channels if the perturbing potential is chosen to be periodic), and into the bound

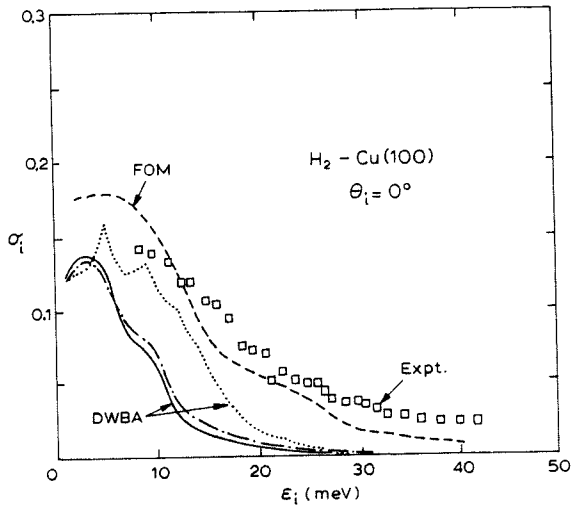

Fig. 9. The sticking coefficient as a function of incident energy for a beam of H_2 incident normally on a Cu(100) surface. The solid line is the DWBA calculation, the dash–dot curve is with all two-phonon contributions. The experimental points are from ref. [32] as well as the dotted curve for the DWBA and the dashed curve for the forced oscillator model.

states. Following the above discussion, the last term is proportional to the sticking coefficient. Therefore, if the sticking has a maximum for a given set of incident conditions, the sum of intensities in the elastic and inelastic channels should be a minimum. Thus one can immediately link extrema found in the sticking coefficient to structure in the inelastic and elastic intensities.

We have carried out a study of the sticking coefficient of H_2, D_2 and Ne at metal surfaces using the theoretical methods described here [34], and we present a few of the pertinent results. The potential used for the calculations is the vibrationally corrugated exponential repulsion representing the repulsive exchange forces near the surface, together with an attractive part as discussed above in eq. (6.1). Two different choices were made for the attractive potential. The exponential attractive part of eq. (6.3) which produces the Morse potential has the advantage that all necessary matrix elements are obtainable in closed form. We have also carried out calculations for which the exponential attractive potential is smoothly joined to a potential of the form $-C_3/z^3$ in the asymptotic region. In this latter case the matrix elements must be calculated entirely numerically, and in fact, we found very little difference between the results produced by the two different attractive forms. Calculations have been carried out for the distorted wave Born approximation, and for terms of higher order in distorted wave perturbation theory, including all terms of single- and double-phonon transfers (which includes terms through fourth order).

Some results for the sticking of molecular hydrogen scattered by the copper (100) face are shown in fig. 9. The sticking coefficient σ_i is plotted as a function of incident energy, and the theoretical calculations are compared with the experimental data [32]. The calculations are shown for both the distorted wave Born approximation, and with all higher-order terms with corrections due to double-phonon exchange. Also shown in fig. 9 are two different calculations of Andersson et al. for the distorted wave Born approximation and the forced harmonic oscillator model [32]. The distorted wave Born approximation of Andersson et al. shows some sharp structure in σ_i at low energies, which arises directly from a sharp structure in their phonon spectral density. This structure is not apparent in our calculations because we use the phonon spectral density of four surface atoms, as has been shown to be necessary for describing scattering into the continuum [22,26,28]. This structure also does not appear in the forced oscillator model of Andersson et al.

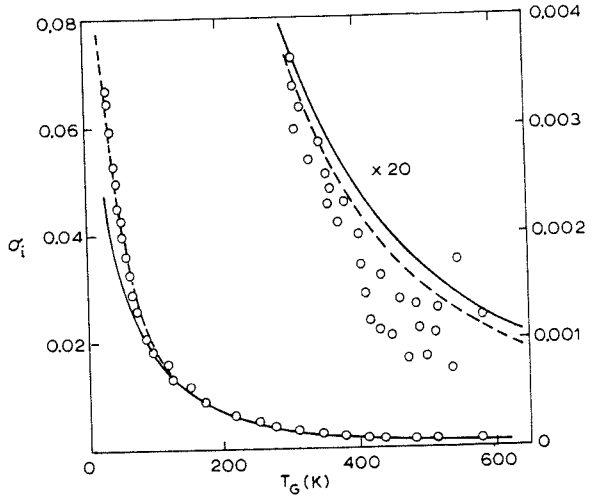

Fig. 10. The sticking coefficient of Ne on Ru(100) for the experimental conditions of ref. [33] as a function of incident gas temperature. The points are a representative sample of the data, the dashed line is the calculation of ref. [33], and the solid line is the present calculation.

Our calculated curves lie somewhat below the experimental points. They could be made to lie much closer to the experimental points by decreasing the number of surface atoms over which the phonon spectral density is calculated. However, we have chosen to retain the same spectral density that has proven to be satisfactory for previous calculations.

A very interesting feature of our calculations is that, viewed as a function of increasing energy, σ_i initially has a maximum and then shows a globally decreasing behavior, but with some clearly superimposed oscillations of small amplitude. The origin of these oscillations is the fact that each different bound state contributes most strongly to the sticking at a different incident energy. As a function of increasing incident energy each bound state contribution rises to a single maximum and then decreases. The maximum contribution to σ_i comes from the bound state levels in the middle, with the highest and lowest levels contributing very little. However, the position of the maximum for each bound state contribution increases in energy with the order of the state, and the oscillations in the sticking coefficient of fig. 9 can be directly related to the maxima appearing in the individual bound state contributions. The behavior of these oscillations is sufficiently strong that they also appear in the dependence of the specular beam intensity as a function of incident energy. This can be shown either by direct calculation of the specular intensity, or through the use of the unitarity relation of eq. (8.2). Mirror images of the structure in σ_i appear superimposed on the general decreasing intensity of the specular intensity as a function of increasing incident energy.

In fig. 10 we compare the results of calculations with experiment for the sticking of Ne on a Ru(001) surface. In the absence of a precise determination of the Ru–Ne potential, we take in the calculation the potential determined by neon scattering experiments on Cu(100) [35]. This leads us to ascribe to the Morse potential parameters the following values: $D = 12.2$ meV and $\chi = 1.9$ Å^{-1}. Figure 10 gives a comparison with the experimental results for Ne sticking on Ru as a function of incident gas energy by including the energy distribution of the incident beam. For the phonon spectral density of the Ru(001) face we use that of the Cu(001) face corrected for the Ru bulk Debye temperature of 415 K and atomic mass of 101 a.u. For the scattering of He and H_2 from Cu(001) surfaces it has been found necessary to take the spectral density of four surface atoms, and we have done the same for Ru.

The calculations include all two-phonon processes through fourth order in perturbation theory, although the dominant contribution, especially at energies smaller than 10 meV, comes form the single-phonon exchange. The calculated values of the sticking coefficient are practically the same as the experimental data for incident energies larger than 60 K. At lower incident energies there is a small discrepancy that may be due to uncertainty in knowledge of the Ne–Ru interaction potential or in the phonon spectral density. The good agreement with the theory, and the dominance of single quantum energy transfers confirms the quantum mechanical nature of the interaction of Ne with the Ru surface at these energies.

9. Conclusions

We have considered in this review the development of the general methods of transition matrix theory of surface scattering problems, together with numerous applications to experiments using atoms and simple molecules as scattering probes. The development of the general formalism is based heavily on the two-potential formalism of Gell-Mann and Goldberger, and is developed to cover the broad areas of coherent, incoherent and inelastic scattering.

The basic problem is one of solving the many-body Schrödinger equation and both exact and approximate methods have been developed. Only the problem of elastic scattering from a perfectly ordered and periodic rigid potential is sufficiently simple for a exact solution. We have presented here two methods of exactly solving such problems, the summation of the complete perturbation series to arbitrary order, and the direct inversion of the transition matrix equation. These two methods complement the more standard method of the close coupling formalism, and have the distinct advantage that for complex systems with many diffracted beams they are much faster in terms of computer time. Both methods can readily treat resonances with the adsorbed bound states (selective adsorption resonances) using the method of Feshbach projection. These elastic scattering methods have been applied to numerous problems of elastic diffractive scattering from periodic surfaces and investigations of selective adsorption resonances as well as threshold resonances.

The problem of inelastic scattering involves the complete solution for the problem of a projectile interacting with a dynamical many-body target and can be solved only approximately. Our approach is to sum the many-body perturbation series to low order in a manner which accounts for all contributions of a given order in the Bose–Einstein distribution function $n(\omega)$. (At higher temperatures where $n(\omega)$ can be replaced by its first-order expansion $k_b T/\hbar\omega$, this condition is equivalent to calculating all terms through a given order n of T^n.) In addition to calculating lower-order terms in the perturbation series, the method has been developed to include the effects of higher-order terms in the perturbation series through infinite-order resummation of virtual processes (resummation of certain classes of closed-loop Feynman diagrams). These inelastic scattering methods have been applied to the problems of thermal attenuation of elastic diffraction peaks (the Debye–Waller effect), the inelastic intensity and in particular that of the single-phonon exchanges, and the problem of capture and sticking in a physisorbtion potential. From point of view of practical calculations, it is worthwhile to notice that the equivalence between diagrams and analytical expressions of t matrix elements, as well as the deduction of inelastic diagrams from the elastic ones, are very powerful. In our work the enumeration of diagrams has been made by hand. It is certainly possible to achieve this operation on a computer and to deduce an algorithm giving the best resummation procedure.

The final class of problems which has been considered in this review is scattering from disordered surfaces. In common with inelastic scattering, this also is a many-body problem which is too complex for exact solution. We have developed the methods of perturbation theory in the two-potential formalism. Starting with the exact solution for a distorting potential corresponding to an isolated surface defect,

such as an adsorbate, vacancy or step, we have investigated the incoherent scattering of distributions of surface defects. Although this method has as yet only been applied to lower order terms in the distorted wave perturbation series, it is amenable to resummations to all higher orders of several classes of closed-loop diagrams. We have applied these methods to problems of He scattering from adsorbates, surface vacancies and distributions of steps on the surface.

When an incident beam of projectiles is backscattered from a surface, the scattered intensity consists of diffraction peaks arising from periodic surface order, a diffuse elastic intensity from disorder, single quantum inelastic peaks from the exchange of surface-localised excitations such as Rayleigh mode phonons, and a diffuse inelastic background coming from inelastic collisions with defects or from multiquantum exchanges with surface excitations. We have shown that transition matrix methods can be specifically developed to describe theoretically each of these components of the scattered intensity. Numerous comparisons of theory with experimental data confirm that transition matrix methods are a very powerful theoretical tool for treating the interaction of a probe with a surface.

Acknowledgements

The authors would like to express their appreciation for many helpful discussions with J. Lapujoulade, B. Salanon, L. Barbier, and H.-J. Ernst, and address many thanks to N. Auby who has carried out a large part of the programming. The authors would also like to thank C. Boiziau for his continued interest and support. JRM would like to acknowledge support by the NSF through grant no. DMR 9114015.

Appendix

In this work, many expressions to be calculated contain integrals of the type:

$$I(r, p) = \int_0^\infty \frac{f(r, q)}{p^2 - q^2 + i\epsilon}\, dq. \tag{A.1}$$

If p^2 is negative the singularity disappears, the denominator being non-vanishing. The function f is in general a potential matrix element which behaves as $\exp(-\beta q)$ for large values of q. The integral is convergent.

For positive values of the square of the parameter p, the integral becomes

$$I(r, p) = -i\pi \int_0^\infty f(r, q)\ \delta(p^2 - q^2) + P\int_0^\infty \frac{f(r, q)}{p^2 - q^2}\, dq \tag{A.2}$$

or

$$I(r, p) = -i\pi \frac{f(r, p)}{2p} + P\int_0^\infty \frac{f(r, q)}{p^2 - q^2}\, dq, \tag{A.3}$$

where P indicates a principal value integral.

Looking at the Taylor expansion of $f(r, p)$, it is easy to show that the ratio

$$\frac{f(r, q) - f(r, q)}{p^2 - q^2}$$

has no singularity for $q = p$. Therefore the principal value integral can be rewritten as

$$P\int_0^\infty \frac{f(r,q)}{p^2-q^2}\,\mathrm{d}q = \int_0^\infty \frac{f(r,q)-f(r,p)}{p^2-q^2}\,\mathrm{d}q + f(r,p)P\int_0^\infty \frac{\mathrm{d}q}{p^2-q^2}. \tag{A.4}$$

On the right-hand side the principal value integral is equal to zero and the integration reduces to the first term, which is well defined. In numerical calculations the upper limit of integration is a finite number say Q, large compared to the value of p and such that $f(r, Q)$ has very small values. One can write

$$P\int_0^\infty \frac{f(r,q)}{p^2-q^2}\,\mathrm{d}q = \int_0^Q \frac{f(r,q)-f(r,p)}{p^2-q^2}\,\mathrm{d}q + \int_Q^\infty \frac{f(r,q)}{p^2-q^2}\,\mathrm{d}q - f(r,p)\int_Q^\infty \frac{\mathrm{d}q}{p^2-q^2}, \tag{A.5}$$

an expression in which the second integral can be neglected for sufficiently large Q. In fact one tries different greater and greater Q values and retains those which yields a stable result, to the desired precision. Under these conditions the integral is given by:

$$I(r,p) = \left[-\mathrm{i}\pi + \log\left(\frac{Q+p}{Q-p}\right)\right]\frac{f(r,p)}{2p} + \int_0^Q \frac{f(r,q)-f(r,p)}{p^2-q^2}\,\mathrm{d}q. \tag{A.6}$$

The integrals encountered in the calculation of quantities involved in inelastic theory are over the variables Ω and have for limits $\pm\Omega_{\max}$. In these expressions the combination of (A.3) and (A.4) gives the exact result without any difficulty.

All integrals are calculated in using the Gregory algorithm. This is a trapezoidal method with corrections at each extremity of the integration interval. This interval being decomposed into N subintervals Δq, each value of the function to be integrated, say $F(q_n)$, is multiplied by a coefficient $\mathrm{CG}(n)$ equal to 1 except, for instance, at the seven F values of each extremity where they take account of the Gregory corrections. Then one has:

$$\int_0^Q F(q)\,\mathrm{d}q = \Delta q \sum_0^N \mathrm{CG}(n)\,F(q_n), \quad \Delta q = \frac{Q}{N}. \tag{A.7}$$

Thus in the programming each F value is multiplied by a coefficient, the set of coefficients being stored as a vector.

An integral equation, such as eq. (3.10), is transformed in this way into a linear equation. To the whole set of equations corresponds a set of coupled linear equations, which is solved with the help of matrix inversion methods. One achieves some numerical calculations with respectively decreasing and increasing values of Δq and Q, until the physical quantities obtained become stable, to the desired precision.

References

[1] H. Hoinkes, Rev. Mod. Phys. 52 (1980) 933.
G. Boato and P. Cantini, Adv. Electron. Electron Phys. 60 (1983) 95.
J.A. Barker and D.J. Auerbach, Surf. Sci. Reports 4 (1984) 1.
T. Engle and K.H. Rieder, Springer Tracts Mod. Phys. 19 (1982) 1.
[2] V. Bortolani and A.C. Levi, Rivista del Nuovo Cimento 9 (1986) 1.
R.B. Gerber, Chem. Rev. 87 (1987) 29.
V. Celli, in: Many Body Phenomena at Surfaces, eds. by D. Langreth and H. Suhl (Academic, New York 1984).
J.R. Manson, in Helium Atom Scattering from Surfaces, ed. by E. Hulpke Springer Series in Surface Science, Vol. 27 (Springer, Heidelberg, 1992) p 173.

[3] M. Gell-Mann and M.L. Goldberger, Phys. Rev. 91 (1953) 398.
[4] G. Armand, J. Phys. (France) 41 (1980) 1475.
[5] J. Lapujoulade, Y. Lejay and G. Armand, Surf. Sci. 95 (1980) 107.
[6] R.G. Newton, Scattering Theory of Waves and Particles (MacGraw Hill, New York 1966).
[7] G. Wolken, Jr., J. Chem. Phys. 58 (1973) 3047; 59 (1973) 1159.
[8] G. Armand and J.R. Manson, Phys. Rev. Lett. 43 (1979) 1839.
[9] L. Barbier and L. Masson, private correspondence.
[10] G. Armand and J.R. Manson, Surf. Sci. 119 (1982) L299.
[11] G. Armand and J.R. Manson, J. Phys. (France) 44, 473 (1983).
[12] B. Salanon, G. Armand, J. Perreau and J. Lapujoulade, Surf. Sci. 127 (1983) 135.
[13] N. Cabrera and J. Solana, Proc. Intern. School of Physics E. Fermi (Compositori, Bologna, 1974) p. 530.
N. Garcia and W.A. Schlup, Surf. Sci. 122 (1982) L657.
[14] G. Armand and J.R. Manson, Surf. Sci. 169 (1986) 216.
[15] B. Poelsema, S.T. de Zwart and G. Comsa, Phys. Rev. Lett. 49 (1982) 578.
[16] H. Wilsch and K.H. Rieder, J. Chem. Phys. 78 (1983) 7491.
[17] G. Armand and B. Salanon, Surf. Sci. 217 (1989) 317.
[18] G. Armand and B. Salanon, Surf. Sci. 217 (1989) 341.
[19] G. Armand, to be published.
[20] G. Armand, J. Phys. (France) 50 (1989) 1493.
[21] L. Van Hove, Phys. Rev. 95 (1954) 249.
[22] G. Armand and J.R. Manson, Phys. Rev. Lett. 53 (1984) 1112.
[23] G. Armand and J.R. Manson, Dynamics on Surfaces, eds. B. Pulmann et al. (Riedel, Dordrecht, 1984) p. 59.
[24] G. Armand, J.R. Manson and C.S. Jayanthi, J. Phys. (France) 47 (1986) 1357.
[25] G. Armand, J.R. Manson and C.S. Jayanthi, Phys. Rev. B 34 (1986) 6627.
[26] G. Armand, J. Lapujoulade and Y. Lejay, Surf. Sci. 63 (1977) 143.
[27] G. Armand, J. Phys. (France) 38 (1977) 989.
[28] G. Armand, D. Gorse, J. Lapujoulade and J.R. Manson Europhys. Lett. 3 (1987) 113.
[29] J.R. Manson and G. Armand, Surf. Sci. 184 (1987) 511.
[30] J.R. Manson and G. Armand, Surf. Sci. 195 (1988) 513.
[31] G. Armand and J.R. Manson, Phys. Rev B 37 (1988) 4363.
[32] S. Andersson, L. Wilzén, M. Persson and J. Harris, Phys. Rev. 40 (1989) 8146.
[33] H. Schlichting, D. Menzel, T. Brunner, W. Brenig and J.C. Tully, Phys. Rev. Lett. 60 (1988) 2515.
[34] G. Armand and J.R. Manson, Phys. Rev. B 43 (1991) 14371.
[35] B. Salanon, J. Phys. (France) 45 (1984) 1373.